

First-Passage-Time Prototypes for Precipitation Statistics

SAMUEL N. STECHMANN

Department of Mathematics, and Department of Atmospheric and Oceanic Sciences, University of Wisconsin—Madison, Madison, Wisconsin

J. DAVID NEELIN

Department of Atmospheric and Oceanic Sciences, University of California, Los Angeles, Los Angeles, California

(Manuscript received 29 August 2013, in final form 27 December 2013)

ABSTRACT

Prototype models are presented for time series statistics of precipitation and column water vapor. In these models, precipitation events begin when the water vapor reaches a threshold value and end when it reaches a slightly lower threshold value, as motivated by recent observational and modeling studies. Using a stochastic forcing to parameterize moisture sources and sinks, this dynamics of reaching a threshold is a first-passage-time problem that can be solved analytically. Exact statistics are presented for precipitation event sizes and durations, for which the model predicts a probability density function (pdf) with a power law with exponent $-3/2$. The range of power-law scaling extends from a characteristic small-event size to a characteristic large-event size, both of which are given explicitly in terms of the precipitation rate and water vapor variability. Outside this range, exponential scaling of event-size probability is shown. Furthermore, other statistics can be computed analytically, including cloud fraction, the pdf of water vapor, and the conditional mean and variance of precipitation (conditioned on the water vapor value). These statistics are compared with observational data for the transition to strong convection; the stochastic prototype captures a set of properties originally analyzed by analogy to critical phenomena. In a second prototype model, precipitation is further partitioned into deep convective and stratiform episodes. Additional exact statistics are presented, including stratiform rain fraction and cloud fractions, that suggest that even very simple temporal transition rules (for stratiform rain continuing after convective rain) can capture aspects of the role of stratiform precipitation in observed precipitation statistics.

1. Introduction

Cloud and precipitation processes are initiated at a natural threshold when water vapor reaches a saturation value. In addition, clouds and precipitation involve turbulent variability that can often be modeled stochastically. Taken together, a stochastic process with a threshold is a first-passage-time problem (Redner 2001; Gardiner 2004). The main purpose of this paper is to present first-passage-time prototype models for precipitation and water vapor statistics. A key aspect of the models here is that they are exactly solvable.

Thresholds arise in various ways in conjunction with clouds and precipitation. On small scales, for instance,

the Clausius–Clapeyron equation provides a threshold for saturation. In large-scale models, convective parameterizations include a threshold for convective onset, such as the one used by the Betts–Miller adjustment scheme (Betts 1986).

In recent studies, a threshold has been identified empirically for the transition to strong convection as a function of bulk environmental variables such as column water vapor (CWV) and tropospheric vertical-average temperature, on scales of $O(20)$ km or larger, as summarized in Fig. 1a. When CWV is below the threshold, mean precipitation is small, and when CWV exceeds the threshold, mean precipitation increases rapidly. Peters and Neelin (2006) noted that in certain respects the threshold resembles a critical point in statistical physics terminology, and used this well-studied prototype for statistics of ensembles of interacting elements near a transition, along with related self-organized criticality prototypes (Christensen and Moloney 2005), to suggest

Corresponding author address: Samuel N. Stechmann, University of Wisconsin—Madison, Department of Mathematics, 480 Lincoln Dr., Madison, WI 53706.
E-mail: stechmann@wisc.edu

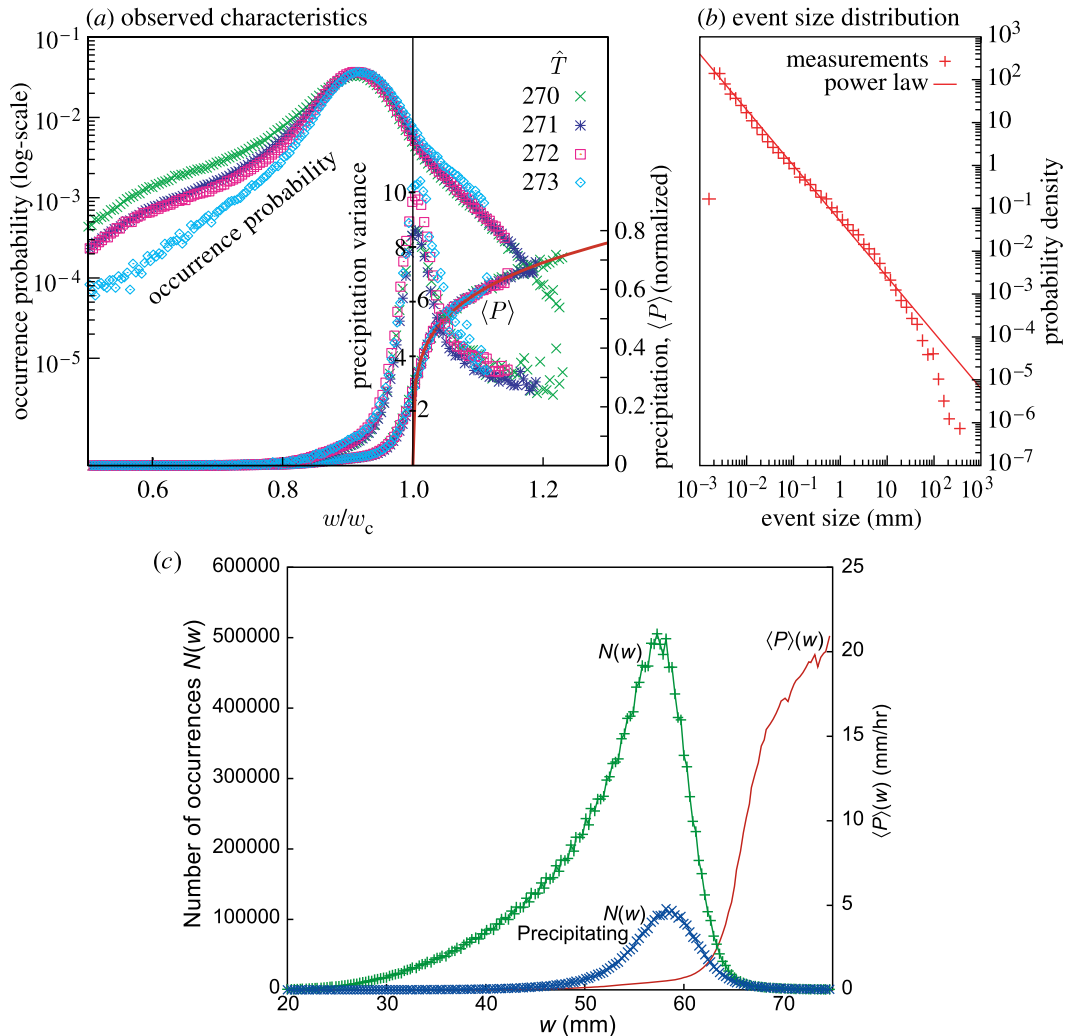


FIG. 1. Summary of observational analyses of the transition to strong convection. (a) Mean precipitation, variance of precipitation, and CWV pdf (for precipitating points) from microwave retrievals (Hilburn and Wentz 2008) as functions of CWV (scaled by the empirical critical value for each tropospheric temperature). The different symbols correspond to data for different values of vertically averaged tropospheric temperature \hat{T} . The vertical black line denotes the critical CWV value. Note that CWV is denoted by w in this figure, whereas it is q in the rest of the paper. (b) Distribution of precipitation event sizes (from optical gauge data). The solid line indicates a power-law fit. From Neelin et al. (2008). (c) CWV pdf for all points (green) and for precipitating points (blue), and mean precipitation (red) as a function of CWV. The critical CWV value here is roughly 65 mm. From Peters and Neelin (2006).

a set of properties to examine in observations. These include power-law ranges in spatial and temporal correlation and in event-size distributions (Peters et al. 2001, 2010); see Fig. 1b. Furthermore, the “critical point” is similar to the equilibrium state envisioned by the theory of convective quasi equilibrium (Arakawa and Schubert 1974), in that it is associated with the onset of conditional instability (Holloway and Neelin 2009), and the resulting dissipation of entraining convective available potential energy above critical results in probability density functions (pdfs) of CWV for precipitating points that peak just below the critical point (Figs. 1a,c).

Such statistics can potentially serve to constrain or improve convective parameterizations in general circulation models (GCMs) (Neelin et al. 2008). For this, it can be useful to have more precise prototype models that relate directly to the equations of atmospheric models and that can explicitly examine how such pdfs arise, including contributions of large-scale and subgrid-scale processes.

To this end, Stechmann and Neelin (2011, hereafter SN11) designed a simple stochastic model for the evolution of CWV and precipitation. In that model, a prognostic equation for CWV was driven by stochastic forcing representing large-scale moisture convergence

and (in the precipitating state) a stochastic contribution to precipitation, and furthermore a stochastic threshold was used: when CWV reaches the critical value, precipitation is allowed to begin with some probability, but it does not necessarily begin precisely at the critical value. This stochastic threshold was motivated by the statistical nature of the observed threshold (Neelin et al. 2009) and by earlier use of stochastic jump processes for parameterizing convective transitions (Majda and Khouider 2002; Majda and Stechmann 2008). At the critical value of CWV, the model of SN11 reproduced the transition in mean precipitation and the peak in precipitation variance. The mean and variance are also captured by the model of Muller et al. (2009), which uses a simpler setup that neglects evolution in time but does consider stochastic effects in the presence of an onset boundary. In the time-evolving model of SN11, the additional statistics in Fig. 1 were also reproduced, including the pdf of CWV and the distribution of precipitation event sizes.

To better understand some of the processes that are captured numerically in SN11, the model presented here uses a number of simplifications including a fixed threshold rather than a stochastic threshold. While this simplification may come at the expense of some realism, it allows analytical solutions to be found. Consequently, errors from statistical sampling of Monte Carlo realizations are absent, and exact statistics can be presented unambiguously. Furthermore, interesting relationships are revealed by comparing formulas for different statistics. For example, the same characteristic CWV value, P_*/D_1^2 , will appear as an important element of both the precipitation-event-size distribution and the CWV pdf; and, in addition, this characteristic value is related to a precipitation rate P_* and a water vapor forcing variance D_1^2 . Through these statistical relationships and this type of insight, the present paper is aimed at two questions: What is the simplest prototype model for precipitation and water vapor statistics? What does the model reveal about the underlying physical processes?

Among the various types of rainfall models in existence, the models presented here are most similar to those that use renewal processes (Cox 1962; Green 1964; Roldán and Woolhiser 1982; Foufoula-Georgiou and Lettenmaier 1987; Schmitt et al. 1998; Bernardara et al. 2007), although many of these previous models apply to daily precipitation, whereas the present focus includes subdaily time scales. A distinguishing feature of the present paper is that the renewal process for precipitation events is not an isolated process; rather, it arises from the dynamics of the water vapor.

Furthermore, regarding precipitation–water vapor relationships, the models here are aimed at the suite of observational analyses (Peters and Neelin 2006; Neelin

et al. 2009) summarized above. In providing tractable solutions that imitate this set of properties in a first-passage setting, it should be possible to make more precise statements about the relationship of the convective transition to properties of self-organized criticality (Peters and Neelin 2006; Christensen and Moloney 2005), which can sometimes be described in terms of first-passage problems (Redner 2001; Sornette 2004). Further studies of these topics have been undertaken with cloud-resolving models (Yano et al. 2012; S. K. Krueger and A. K. Kochanski 2013, personal communication). In the present study, by reproducing a suite of the observed statistics in an exactly solvable model, the aim is to better understand the underlying physical processes. An aspect of particular interest is the distribution of sizes of precipitation events (Peters et al. 2001, 2010). As shown in Fig. 1b, the event-size distribution follows a power law over a wide range of event sizes. As a further surprise, similar event-size distributions are seen at many locations around the world, despite major differences in their local climates. This universality suggests that, even across a wide range of climates, some common aspects exist in disparate classes of precipitation events.

The partitioning of precipitation into deep convective and stratiform components has long been investigated (Cheng and Houze 1979; Steiner et al. 1995; Short et al. 1997; Rickenbach and Rutledge 1998; Schumacher and Houze 2003; Yuter et al. 2005). The importance of this partitioning is multifaceted; as one example, these components have different profiles of vertical heating, which has important consequences for atmospheric dynamics (Houze 1989; Mapes 1993, 2000; Schumacher et al. 2004; Khouider and Majda 2006; Tulich et al. 2007; Khouider and Majda 2008; Majda and Stechmann 2009; Stechmann and Majda 2009). One of the models in the present paper will include these two components—deep convective and stratiform—and will have exactly solvable statistics for stratiform rain fraction and convective rain fraction. This permits examination in the temporal domain of the role transitions to and from stratiform precipitation can play near the critical point of Fig. 1.

In short, the aim here is to ask what aspects of the observed statistics can be imitated in a model that only contains time evolution of column-integrated water vapor and simple onset thresholds that switch among precipitation states, including a dependence on the direction of the threshold is crossed. In the two-state model, there is a nonprecipitating state in which an evaporation-like source term creates an upward drift in moisture toward the precipitation onset threshold, and a precipitating state in which precipitation creates a drift toward lower moisture, with the cessation of

precipitation occurring at a slightly smaller value than the onset threshold. In both states, moisture convergence and/or divergence by fluctuating large-scale dynamics is represented by a stochastic term. In the three-state model, the consequences of distinguishing between a deep convective and a stratiform precipitating state are analyzed, with the stratiform state occurring within a certain range as moisture decreases from the deep convective state. In observations or three-dimensional models, there can be spatial interactions that potentially affect evolution in realistic states corresponding to these. The analysis here indicates the statistics for a fairly extensive set of phenomenon can be at least qualitatively captured with simple time-evolution rules.

A complementary relationship may be noted to advection–condensation models or time-of-last-saturation analysis (e.g., Pierrehumbert 1998; Galewsky et al. 2005; O’Gorman and Schneider 2006; Pierrehumbert et al. 2007; Sukhatme and Young 2011; O’Gorman et al. 2011). These examine the pdf or other statistics of water vapor—for instance, under stochastic advection on an isentropic surface—taking the last saturation as a boundary at which the humidity is set to saturation. Here, evolution is similarly driven by a stochastic representation of advection effects, but the threshold corresponds to the onset of conditional instability in the column, rather than to saturation, and thus water vapor can continue to exhibit nontrivial dynamics in the interval above the threshold. Quantities of interest thus include statistics such as the pdfs of precipitating points on both sides of the threshold and event-size distributions. Evolution on the nonprecipitating side is analogous to the advection–condensation models. For instance, Pierrehumbert et al. (2007) note a scaling range for the distribution of intervals between encounters with the saturation boundary that corresponds to that found for dry spells in the present model.

The paper is organized as follows. In sections 2–4, a two-state model is presented for convective onset and shutdown. After the model description in section 2, the distributions of event sizes and durations are presented in section 3, and further statistics are presented in section 4. In section 5, a three-state model is presented that partitions precipitation events into deep convective and stratiform episodes. Discussion and conclusions follow in sections 6 and 7, and the appendixes describe some of the calculations.

2. Two-state model for convective onset

In this section a two-state model is presented for onset and shutdown of convective events. The two states are wet spells and dry spells, where the wet spells are times

TABLE 1. Parameters for the two-state model for convective onset.

Symbol	Description	Value
P_*	Precipitation rate	3 mm h ⁻¹
E_*	Evaporation rate	0.4 mm h ⁻¹
D_1^2	Forcing variance ($\sigma = 1$)	64 mm ² h ⁻¹
D_0^2	Forcing variance ($\sigma = 0$)	8 mm ² h ⁻¹
q_c	Critical CWV	65 mm
q_{np}	Low-threshold CWV	62 mm
b	$q_c - q_{np}$	3 mm

of precipitation. This is the simpler of the two prototype models considered here.

The model involves the stochastic evolution of the water vapor $q(t)$ for a single atmospheric column. The dynamics of $q(t)$ depends on whether the column is nonprecipitating or precipitating:

$$\frac{dq}{dt} = E_* + D_0 \dot{\xi} \quad \text{if nonprecipitating,} \quad (1)$$

$$\frac{dq}{dt} = -P_* + D_1 \dot{\xi} \quad \text{if precipitating.} \quad (2)$$

Here $\dot{\xi}$ is Gaussian white noise, E_* is a constant “evaporation” rate, P_* is a constant precipitation rate, and D_0 and D_1 are constants that measure the variance of water vapor forcing. While E_* is referred to as an evaporation rate for simplicity, it represents a mean moisture source due to all relevant processes, such as surface fluxes and moisture advection. Similarly, P_* is the net moisture sink in the precipitating state and so strictly speaking would be precipitation minus evaporation and mean moisture convergence. For simplicity, we discuss it as a precipitation rate here. While it is a crude simplification to treat these moisture sources and sinks as constants, it will allow analytic solutions, and it can be evaluated a posteriori by comparing the statistics from the model and observations.

The values of the model parameters are listed in Table 1. At the moment, the parameter values are chosen based on a comparison between observed statistics and exact theoretical statistics, the latter of which is presented below. In the future, it would be interesting to directly estimate these parameters from observations or model data.

Whether the column is precipitating or nonprecipitating is determined by two thresholds, as illustrated in Fig. 2. If the column is nonprecipitating and $q(t)$ increases to the critical value q_c , then precipitation begins. The dynamics of $q(t)$ switches from (1) to (2). The column remains in the precipitating state until $q(t)$ decreases to a different, lower threshold q_{np} . Upon reaching q_{np} , the column is nonprecipitating again, and the cycle repeats:

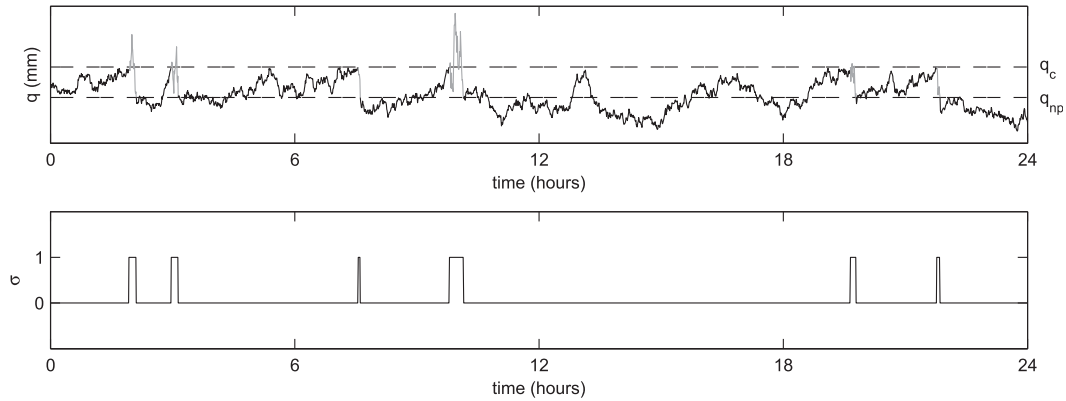


FIG. 2. Sample time series of (top) CWV $q(t)$ and (bottom) precipitation indicator $\sigma(t)$ for 24 h. Dashed lines in the top panel denote the threshold values q_c and q_{np} . Water vapor is shown in black during dry spells and in gray during wet spells.

$$\begin{aligned}
 \frac{dq}{dt} &= E_* + D_0 \dot{\xi} \quad \text{until } q = q_c, \\
 \frac{dq}{dt} &= -P_* + D_1 \dot{\xi} \quad \text{until } q = q_{np}, \\
 \frac{dq}{dt} &= E_* + D_0 \dot{\xi} \quad \text{until } q = q_c, \\
 \frac{dq}{dt} &= -P_* + D_1 \dot{\xi} \quad \text{until } q = q_{np}, \\
 &\vdots
 \end{aligned}
 \tag{3}$$

To keep track of the state of the column as nonprecipitating or precipitating, an indicator variable $\sigma(t)$ is assigned the value of 0 or 1, respectively:

$$\begin{aligned}
 \text{nonprecipitating } \sigma(t) &= 0 \quad \text{until } q = q_c, \\
 \text{precipitating } \sigma(t) &= 1 \quad \text{until } q = q_{np}, \\
 \text{nonprecipitating } \sigma(t) &= 0 \quad \text{until } q = q_c, \\
 \text{precipitating } \sigma(t) &= 1 \quad \text{until } q = q_{np}, \\
 &\vdots
 \end{aligned}
 \tag{4}$$

Notice that knowledge of $q(t)$ alone is not always sufficient to determine whether the column is precipitating or nonprecipitating. If CWV is in the intermediate range $q_{np} < q < q_c$ between the two thresholds, the column could be either precipitating or nonprecipitating, and it is the variable $\sigma(t)$ that records the “memory” of whether the column is precipitating.

Also notice that it is possible for $q(t)$ to increase beyond q_c during a precipitation event, despite P_* . This can happen if the stochastic source–sink term $D_1 \dot{\xi}$, which can be either positive or negative, overcompensates for the loss due P_* ; see Fig. 2 at roughly time $t = 10$ h for an example. In nature, such a strong

moisture source would typically be due to moisture convergence that is crudely represented here by $D_1 \dot{\xi}$. SN11 identified such excursions of $q(t) > q_c$ with the longest-lasting precipitation events in their model. They also identified a portion of the source–sink term with the precipitation process itself; for the sake of analytic solutions in certain precipitation statistics this is omitted here (although it is a straightforward extension for many aspects of the model).

One of the main differences between this model and the model of SN11 is that here precipitation events always start immediately when $q(t)$ increases to q_c and always end immediately when $q(t)$ decreases to q_{np} . In contrast, in the model of SN11, the start and end of precipitation events were governed by a stochastic jump process. The model in (3) can be viewed as a limiting case of the model of SN11: in the limit that the stochastic jump rates become infinite, the system transitions immediately when the threshold q_c or q_{np} is reached.

A second difference from the model of SN11 is that P_* and D_1 are constants in (1) and (2). In contrast, in the model of SN11, $P_*(q)$ and $D_1(q)$ were taken to be q -dependent functions as a way to allow both intense and moderate stages of a precipitation event, to represent deep convective and stratiform rainfall, respectively. Later, in section 5, a three-state model is presented that includes both deep convective and stratiform precipitation. As a simpler prototype, the two-state model in (1) and (2) is presented here first, and it will already display many of the main desired features. Its precipitation rate of $P_* = 3 \text{ mm h}^{-1}$ is meant to be an average or typical precipitation rate during precipitation events (i.e., much higher than the long-term average precipitation rate), characteristic of neither deep convection nor stratiform precipitation exclusively, yet closer to characteristics of stratiform precipitation (Nesbitt et al. 2006).

We note that in SN11 numerical tests of corresponding simplifications were carried out; these identified the features maintained in this model as able to capture key properties such as the power-law range in the event-size distribution. These two simplifications allow exact analytic calculation of the precipitation and water vapor statistics, as shown below.

3. Event-size pdf

An interesting statistic to consider is the event size, which is defined as the total amount of precipitation (mm) to fall during a precipitation event. Observational analyses have shown that small events are most probable and that the distribution of event sizes decays like a power law (Peters et al. 2001, 2010). See Fig. 1 for a reproduction of observational analysis.

For the two-state model, the event size is proportional to the event duration, with proportionality constant P_* . Furthermore, the distributions can be found analytically.

a. Analytic solution

The pdf $p_{t1}(t)$ of precipitation event durations comes from solving the following first-passage-time problem: given that q is initially at the critical value $q = q_c$ at the start of the event, how long does it take q to decrease to the low threshold q_{np} ? The pdf for the event durations is

$$p_{t1}(t) = \frac{b}{\sqrt{2\pi D_1^2}} \exp\left(\frac{P_* b}{D_1^2}\right) \exp\left(-\frac{b^2}{2D_1^2 t}\right) \exp\left(-\frac{P_*^2 t}{2D_1^2}\right) t^{-3/2}, \quad (5)$$

where $b = q_c - q_{np}$. The derivation is given in the appendix. Similarly, the distribution $p_{t0}(t)$ of dry-spell durations is

$$p_{t0}(t) = \frac{b}{\sqrt{2\pi D_0^2}} \exp\left(\frac{E_* b}{D_0^2}\right) \exp\left(-\frac{b^2}{2D_0^2 t}\right) \exp\left(-\frac{E_*^2 t}{2D_0^2}\right) t^{-3/2}. \quad (6)$$

These distributions have a common form with a triple product of (i) a short- t cutoff function $\exp(-t/\tau_{\text{short}})$, (ii) a long- t cutoff function $\exp(-t/\tau_{\text{long}})$, and (iii) a power law $t^{-3/2}$ that holds in between the short- t and long- t cutoffs. Figure 3 shows plots of these distributions on a logarithmic scale to emphasize these features.

Precipitation event size s is proportional to event duration t as $s = P_* t$, since the precipitation rate takes

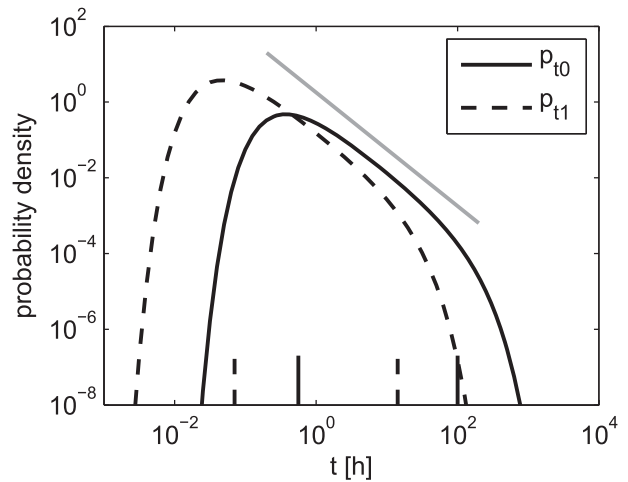


FIG. 3. Event-duration pdf for the two-state model for convective onset. The dry-spell pdf $p_{t0}(t)$ is shown by the solid black line, and the wet-spell pdf $p_{t1}(t)$ is shown by the dashed black line. The gray line shows the power law $t^{-3/2}$. Logarithmic scaling is used on both axes. Formulas for these pdfs are shown in (5) and (6). In the bottom of the plot, the vertical line segments mark the short- t and long- t cutoffs of the power-law ranges, whose formulas are given in (9)–(12); solid and dashed line segments correspond to the solid and dashed pdf curves, respectively.

the constant value P_* in this simple model. As a result, the pdf p_S for event size has essentially the same functional form as the event-duration pdf p_{t1} and is given by

$$p_S(s) = \frac{1}{P_*} p_{t1}\left(\frac{s}{P_*}\right) = C \exp\left(-\frac{s_S}{s}\right) \exp\left(-\frac{s}{s_L}\right) s^{-3/2}, \quad (7)$$

where the normalization constant is

$$C = b[P_*/(2\pi D_1^2)]^{1/2} \exp(P_* b/D_1^2) = (s_S/\pi)^{1/2} \exp[2(s_S/s_L)^{1/2}] \quad (8)$$

and the small- and large-event cutoffs (s_S and s_L) are given below.

b. Cutoffs

In the wet- and dry-spell durations in (5) and (6), the short- t and long- t cutoffs are defined in terms of the model parameters as

$$\text{wet spells: short-}t \text{ cutoff} = \frac{b^2}{2D_1^2}, \quad (9)$$

$$\text{long-}t \text{ cutoff} = \frac{2D_1^2}{P_*^2}, \quad (10)$$

$$\text{dry spells: short-}t \text{ cutoff} = \frac{b^2}{2D_0^2}, \quad (11)$$

$$\text{long-}t \text{ cutoff} = \frac{2D_0^2}{E_*^2}. \quad (12)$$

For the parameters in Table 1, the power-law ranges are then approximately given by

$$\text{wet spells: } 0.070 < t < 14 \text{ h}, \quad (13)$$

$$\text{dry spells: } 0.56 < t < 100 \text{ h}. \quad (14)$$

These cutoffs are indicated in Fig. 3 by the vertical line segments in the bottom of the plot.

While the pdfs for wet- and dry-spell durations have the same functional form, there is a clear asymmetry between them: dry spells last longer than wet spells. A simple quantification of this is in (13) and (14): the dry-spell cutoffs are roughly 10 times longer than the wet-spell cutoffs. This is roughly in agreement with the observational analyses of Peters et al. (2010) and similar to the analysis of daily data by Ratan and Venugopal (2013). In the model here, the asymmetry can be related to the model parameters. In (9)–(12), the exponential cutoffs are related to characteristic time scales in terms of the threshold separation, $b = q_c - q_{np}$; the variances, D_0^2 and D_1^2 ; and the mean source and sink, E_* and P_* . However, the ratios of the dry and wet cutoffs are independent of b . For the short-time cutoffs, the ratio is D_1^2/D_0^2 ; hence the cutoff for dry spells is longer because the variance is smaller. Similarly, for the long-time cutoffs, the ratio is $(P_*^2/E_*^2)/(D_1^2/D_0^2)$; hence the cutoff for dry spells is longer because P_*^2/E_*^2 is even larger than D_1^2/D_0^2 .

Since p_s is related to p_{t1} as shown in (7), its cutoff time scales are related to characteristic water vapor values as well. The relationship is a direct proportionality, with P_* as the proportionality constant, which leads to

$$\text{precipitation event sizes: small-}s \text{ cutoff} = \frac{b^2 P_*}{2D_1^2}, \quad (15)$$

$$\text{large-}s \text{ cutoff} = \frac{2D_1^2}{P_*}, \quad (16)$$

where the precipitation event size is measured in millimeters. For the parameters in Table 1, the power-law range is then approximately given by

$$\text{precipitation event sizes: } 0.21 < s < 42 \text{ mm}. \quad (17)$$

In (15) and (16), notice that the same characteristic water vapor scale, D_1^2/P_* , appears in the expressions for both the small- s and large- s cutoffs. Furthermore, as shown below, this same characteristic scale appears in the water vapor pdf as well.

To summarize, the pdfs of event duration and event size have power-law scaling with exponent $-3/2$. However, this scaling only holds over a finite range of durations and sizes. Outside the power-law range, exponential scaling is seen. In combination, these features characterize the extreme events in this model. Not only does D_1^2/P_* appear as the cutoff between power-law and exponential scaling, but it also is the decay rate of the exponential scaling for large events. This characteristic scale is a ratio of the water vapor forcing variance and precipitation rate, and it is the first of many statistical relationships that will be suggested by the models.

c. Heuristic scaling

Why does the exponent $-3/2$ arise? And why is the exponent independent of all model parameters? The following heuristic argument addresses these questions in relation to probability flux. In brief, probability density is proportional to $t^{-1/2}$, and probability flux inherits an addition factor of t^{-1} and is proportional to $t^{-3/2}$.

Consider the simpler case with $P_* = 0$ and without thresholds. For this case, given $q = 0$ initially, the probability density at a later time is $(2\pi D_1^2 t)^{-1/2} \exp[-q^2/(2D_1^2 t)]$, which is a Gaussian function with variance $D_1^2 t$. From this function, the probability flux is obtained by Fick's law and is proportional to the derivative with respect to q —that is, it is proportional to $-(D_1^2 t)^{-3/2} (q/\sqrt{2\pi}) \exp[-q^2/(2D_1^2 t)]$. This is the power law with exponent $-3/2$. What is the connection between the flux and the first-passage-time problem? By definition, the flux indicates the probability that point q is being passed at time t , and this is essentially the same as the probability that a threshold is passed.

This heuristic argument indicates how the $-3/2$ exponent arises and how it is related to probability flux. See the appendix for a proper derivation including precipitation and a true threshold.

d. Mean and second moment of event-size distribution

The mean and second moments of the event-size distribution are

$$\langle s \rangle = b, \quad (18)$$

$$\langle s^2 \rangle = b \frac{D_1^2}{P_*} + \langle s \rangle^2. \quad (19)$$

The second moment diverges as expected as the large-event-size cutoff goes to infinity—for example, for large D_1^2 or small P_* . An interesting illustration of the usefulness of a physically based prototype is that the mean remains finite in this limit. This is contrary to expectations

for a power law with exponent between -1 and -2 , such as the first-passage time in the limit as drift goes to zero (Redner 2001, p. 84). Indeed, the mean duration diverges as $D_1^2 P_*^{-1}$ in this limit in the two-state model, but the normalization for the event size includes the drift rate P_* in such a way that the mean event size remains finite. To see directly from the equations why this must occur, consider a time integral of (2) in the precipitating regime. Over the duration of an event, the dq/dt term integrates to $-b$, while the event size comes from $\int (-P_*) dt$. If one further takes an expectation over all event sizes, the $D_1 \xi$ term drops out, yielding the mean event size above.

The characteristics of the event-size distribution can change in a way that is independent of the mean precipitation for the model, which is set by long-time average budget considerations and thus depends only on $P_* E_*/(P_* + E_*)$ (see section 4). If moisture convergence variability, measured by D_1^2 , becomes large compared to the P_* and E_* drift terms, a long power-law range and large event-size variance can result even for fixed mean rainfall.

As background for comparison to observations, the two-state model ratio of first and second moments is

$$\frac{\langle s^2 \rangle}{\langle s \rangle} = \frac{D_1^2}{P_*} + b \approx \frac{D_1^2}{P_*} \alpha s_L. \quad (20)$$

This ratio for observational distributions in Peters et al. (2010) was taken as an indicator of the large- s cutoff and used to rescale event size at each of several instrument locations. The two-state model confirms the usefulness of this procedure while suggesting that $(\langle s^2 \rangle - \langle s \rangle^2)/\langle s \rangle$ might be a slightly better measure.

In observations, the very-small-event-size portion of the distribution is typically not reliably observed owing to finite observation intervals and instrumentation error at low rain rates. While in nature a small-event-size cutoff might be affected by many processes including temporal autocorrelation, the two-state model provides a succinct case to examine potential impacts of not observing the cutoff regime. Consider integrals over an interval of event sizes $[s_1, \infty)$. For the mean,

$$\int_{s_1}^{\infty} s p_S(s) ds = b[1 - \epsilon(s_S, s_L, s_1)], \quad (21)$$

using (7), where ϵ is small in both of the two most relevant cases. First, $\epsilon \rightarrow 0$ for $s_1 \rightarrow 0$ (i.e., the full solution). Furthermore, if we consider s_1 to occur in the power-law range as occurs in the data (i.e., $s_1/s_S \gg 1$), and that there is a well distinguished power-law range [i.e., $(s_S/s_L)^{1/2} \ll 1$], we have

$$\epsilon \approx 2\pi^{-1/2} (s_1/s_L)^{1/2}. \quad (22)$$

Thus, if $(s_S/s_L)^{1/2} \ll 1$, ϵ is small (i.e., the contribution to the integral comes from the large- s end), and omission of values less than s_1 has little direct impact on the mean or higher moments. The normalization is affected, since for $\int_{s_1}^{\infty} p_S(s) ds$, the dominant contribution is from close to s_1 . However, a ratio such as (20) would not be.

e. Relation to observational data

We now turn to the question of how directly the simple prototype can be compared to observations. Peters et al. (2001) found a long power-law range in the event-size distributions observed in radar data, with an exponent of -1.36 while Neelin et al. (2008) estimated an exponent of -1.3 from tropical data. Peters et al. (2010) systematically examined event-size distributions from Atmospheric Radiation Measurement Program data. The power-law range for data from various locations is reasonably well fit by exponents of around -1.2 , although some midlatitude cases yield individual estimates from -1 to -1.4 . Peters et al. (2010) also estimated exponents of around -1.3 for power-law ranges in dry period durations. For wet-spell-event durations, the power-law range was much shorter; they suggested an exponent of around -2 , although examination of their figures suggests that an exponent of -1.5 would not be excluded. Andrade et al. (1998) show figures with dry-spell exponents of around -1.8 and -1.9 , noting a wider range of exponents when examining other locations, and an exponent of about -1.6 for rain duration based on daily data. They discuss fits of both a second power-law range and an exponential to the large-duration cutoff.

In the two-state model as formulated here, wet-period duration and event-size distributions have the same functional form. This places a significant caveat on how detailed the comparison to observations should be, for instance, in terms of the exact value of the exponent. However, the two-state model does suggest that even a very simple system with a threshold for rainfall onset can yield a power-law range with an exponent that is in the range of those noted in observations and arguably lies between typical values of the exponents for the event size and for the duration. It further appears to provide a qualitative explanation for the difference in length of power-law range between the wet- and dry-spell durations. Finally, it is appealing as a prototype for a feature of the observations noted in Peters et al. (2010), in which the exponent remained approximately constant in different regions, while the cutoff changed [with the cutoff value approximately

normalized by the ratio (20)]. The two-state model indicates how the parameters of the system affecting such processes as rain rate and moisture convergence should be expected to most strongly affect the cutoffs at the ends of the power-law range, while the exponent of this range is set by what might be termed geometric considerations (in the state space of the random process).

Regarding the similarity of the observed exponent in different observational regions, including both regions dominated by convective rainfall and those that might have substantial large-scale contributions, the two-state model is simple enough that it can be regarded as a prototype for either regime. The setup has been phrased here in terms of exceeding a column water vapor threshold corresponding to the onset of conditional instability and convective rainfall. However, it could work equally well for q interpreted as total water mixing ratio (including condensate) in a particular layer exceeding a critical value for the onset of aggregation and rainout. The fact that the exponent is independent of the model parameters suggests that while the details of the precipitation process differ in different meteorological regimes, affecting the event-size cutoff, the exponent would simply come from the importance of the threshold process. It is currently not known if climate models can reproduce aspects of the observed event-size distribution. If they can, then this prototype suggests that constraints on model parameters will be associated with correctly producing the changes as a function of the region or meteorological regime in the large-event-size cutoff as measured—for example, by $(\langle s^2 \rangle - \langle s \rangle^2) / \langle s \rangle$.

The simplicity of the two-state model offers advantages, notably analytic solutions, but one might ask what alterations could bring it closer to observations. One obvious aspect is the nature of the noise process, since large-scale moisture convergence has nontrivial temporal autocorrelation as well as two-way interactions with the convective heating. In discrete-time random walk models, introducing a time step and step increment given by a random variable drawn from a power-law distribution can yield exponents between -1.5 and -1 for the first-passage time (Redner 2001, p. 90), so it is plausible that a climate model producing more complex moisture transport “noise” could yield exponents differing from -1.5 . One could further postulate that revised precipitation moisture dependence or inclusion of a stochastic precipitation term could create the distinction between duration and event-size distributions seen in the observations, although the exponent seen numerically in SN11 that

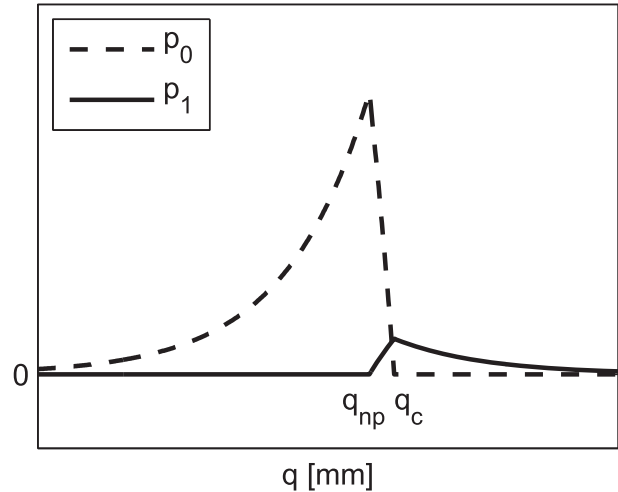


FIG. 4. CWV pdfs for the two-state model for convective onset. The pdf p_1 for the precipitating state is shown with the solid line, and the pdf p_0 for the nonprecipitating state is shown with the dashed line. Formulas for these pdfs are shown in (24)–(27).

included these effects is well explained by -1.5 . Of further interest are the extent to which distributions of various quantities as function of water vapor are reproduced by this model and a simple three-state extension that also admits analytic solutions. This will be addressed in the sections 4 and 5, respectively.

4. Water vapor pdfs, pickup, and variance

In addition to the distributions of event sizes and durations, the stationary pdfs of water vapor and precipitation can be found analytically. These statistics are related to the set of properties of tropical convection summarized in Fig. 1. With the simplifications of the two-state model, we can expect these to be only a rough sketch of the properties captured in SN11, but they can nonetheless provide insight into how much a simple large-scale forcing across a threshold can capture.

The stationary pdfs are denoted $p_0(q)$ and $p_1(q)$, which correspond to the nonprecipitating and precipitating states, respectively. The overall normalization condition is

$$\int [p_0(q) + p_1(q)] dq = 1. \tag{23}$$

By solving a stationary Fokker–Planck equation, as shown in appendix A, one finds that $p_0(q)$ and $p_1(q)$ have a piecewise exponential form, as illustrated in Fig. 4. Explicitly, the formulas are

$$p_0(q) = \frac{1}{b} \frac{P_*}{E_* + P_*} \left[1 - \exp\left(-\frac{2E_*}{D_0^2} b\right) \right] \exp\left[\frac{2E_*}{D_0^2} (q - q_{\text{np}})\right] \quad \text{for } q < q_{\text{np}}, \quad (24)$$

$$p_0(q) = \frac{1}{b} \frac{P_*}{E_* + P_*} \left\{ 1 - \exp\left[\frac{2E_*}{D_0^2} (q - q_c)\right] \right\} \quad \text{for } q_{\text{np}} < q < q_c, \quad (25)$$

$$p_1(q) = \frac{1}{b} \frac{E_*}{E_* + P_*} \left\{ 1 - \exp\left[-\frac{2P_*}{D_1^2} (q - q_{\text{np}})\right] \right\} \quad \text{for } q_{\text{np}} < q < q_c, \quad (26)$$

$$p_1(q) = \frac{1}{b} \frac{E_*}{E_* + P_*} \left[\exp\left(\frac{2P_*}{D_1^2} b\right) - 1 \right] \exp\left[-\frac{2P_*}{D_1^2} (q - q_{\text{np}})\right] \quad \text{for } q_c < q, \quad (27)$$

where $b = q_c - q_{\text{np}}$. These pdfs have the shapes shown in Fig. 4 for essentially any parameter choices with small E_*/P_* and small $q_c - q_{\text{np}}$. The pdf p_0 for nonprecipitating points is similar to that seen in observational analyses: the peak occurs just below q_c , and decay is seen for low CWV values; see Peters and Neelin (2006) as reproduced here in Fig. 1. However, the pdf p_1 for precipitating points is mostly concentrated above q_c , which is not what is seen in the observational analyses shown in Fig. 1; this aspect will be rectified in section 5 by partitioning precipitation into deep convective and stratiform components. In observations and full atmospheric models, the onset of conditional instability for convective plumes will depend on vertical structures not captured by CWV, which will tend to act like a stochastic effect on q_c . It is thus worth noting briefly how a simple case of a stochastic threshold would affect these pdfs. Consider an average over an ensemble of realizations in which q_c has a random component—for example, over an ensemble of spatial points as in the observational analysis (not time varying on the scales considered here, which would require more detailed treatment). This would tend to smooth the pdfs in Fig. 4. While this might somewhat improve the comparison to the pdfs from the microwave retrievals, it would not compare as well as the three-state model or SN11 cases. The rudimentary pdf here serves as a baseline against which to compare these.

It is illuminating to assume a particular column water vapor value q and to examine the precipitation statistics for such a column. This approach has been used by Bretherton et al. (2002) for daily data and Peters and Neelin (2006) and Neelin et al. (2009) for instantaneous retrievals. In the two-state model here, the conditional mean and variance of precipitation are respectively given by

$$\langle \text{precip} \rangle(q) = \frac{P_* p_1(q)}{p_0(q) + p_1(q)}, \quad (28)$$

$$\langle \text{precip}^2 \rangle(q) - \langle \text{precip} \rangle^2(q) = \frac{P_*^2 p_1(q)}{p_0(q) + p_1(q)} - \langle \text{precip} \rangle^2(q). \quad (29)$$

Figure 5 shows plots of these quantities. The critical value marks a rapid increase in mean precipitation, as expected from the model assumptions, and a “foot” of width proportional to D_1^2/P_* leads up to this, associated with the hysteresis of temporal onset and termination. A similar scale appears in SN11 but is strongly modified by the stochastic jump process in that model, and vertical structure variations are not included here, so the two-state representation should be taken as very rough when comparing to the observations in Fig. 1, where a qualitatively similar foot region may be seen below the critical value. For the simplest assumptions, a peak in precipitation variance occurs just below q_c in Fig. 5. If a small portion of $D_1 \xi$ in (2) is taken to be a random component of the precipitation, as in SN11, the precipitation variance above q_c increases accordingly. The microwave retrievals in the high-precipitation range should be treated with due caution, since they are based on cloud water, variance of which may differ from that of surface precipitation, so constraints on the partition of the D_1 term are limited. However, as in SN11, the two-state model makes clear that the important properties, including event-size distributions and pdfs of precipitating points, are essentially independent of this partition.

The precipitating fraction $P\{\sigma = 1\}$ in this model is the fractional time spent in the precipitating state, $\sigma = 1$, and is defined by integrating over all possible water vapor values:

$$P\{\sigma = 0\} = \int_{-\infty}^{q_c} p_0(q) dq, \quad (30)$$

$$P\{\sigma = 1\} = \int_{q_{np}}^{\infty} p_1(q) dq, \quad (31)$$

where the nonprecipitating fraction $P\{\sigma = 0\}$ is defined similarly. These can be computed analytically using (24)–(27), and one finds

$$P\{\sigma = 0\} = \frac{P_*}{E_* + P_*}, \quad (32)$$

$$P\{\sigma = 1\} = \frac{E_*}{E_* + P_*}. \quad (33)$$

Equivalently, one can obtain these from the long-time average of (1) and (2) and $P\{\sigma = 0\} = 1 - P\{\sigma = 1\}$, showing that these are simply set by moisture balance. For the particular parameter values from Table 1, the numerical values are $P\{\sigma = 0\} = 0.88$ and $P\{\sigma = 1\} = 0.12$. Furthermore, the mean precipitation can be computed from these quantities as

$$\langle \text{precip} \rangle = P_* P\{\sigma = 1\} = \frac{P_* E_*}{E_* + P_*}. \quad (34)$$

For the particular parameter values used here, the numerical value is $\langle \text{precip} \rangle = 8.5 \text{ mm day}^{-1}$.

In short, the two-state model is a simple prototype for dynamics of water vapor and precipitation, and its statistics can be found analytically. The formulas offer null hypotheses for many statistical relationships. For example, the exponential decay rate of the water vapor pdf is related to the mean E_* and variance D_0^2 of water vapor forcing as $2E_*/D_0^2$. While not all aspects of the model are in agreement with the observational analyses in Fig. 1, it has efficient explanatory power, and it can be viewed as a null hypothesis against which any more complex model should be compared. In the next section, a more realistic prototype is introduced that partitions precipitation into deep convective and stratiform episodes.

5. Three-state model with stratiform precipitation

In this section a three-state model is presented that not only includes wet spells and dry spells but also partitions wet spells into episodes of deep convective and stratiform precipitation. This will allow additional statistics to be computed, including deep convective and stratiform rain fractions.

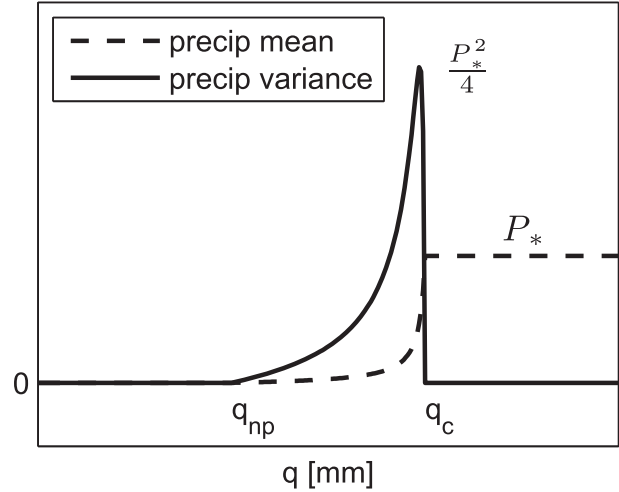


FIG. 5. Precipitation mean (dashed) and variance (solid), conditioned on each CWV value q , for the two-state model for convective onset. Formulas for these conditional statistics are shown in (28) and (29), and their maximum values are indicated in the plot: P_* for the mean and $P_*^2/4$ for the variance. See text for discussion of variance above q_c .

a. Model description

In the three-state model, the dynamics of $q(t)$ depends on whether there is no precipitation, deep convective precipitation, or stratiform precipitation:

$$\frac{dq}{dt} = E_* + D_{np} \xi \quad \text{if nonprecipitating,} \quad (35)$$

$$\frac{dq}{dt} = -P_d + D_d \xi \quad \text{if deep convective,} \quad (36)$$

$$\frac{dq}{dt} = -P_s + D_s \xi \quad \text{if stratiform.} \quad (37)$$

Here the constants P_d and P_s are the deep convective and stratiform precipitation rates, respectively, and D_d^2 and D_s^2 are the water vapor forcing variances for those two states (parameter settings will be discussed below).

The state of the column—nonprecipitating, deep convection, or stratiform—is determined by three thresholds, as illustrated in Fig. 6. As before, q_c and q_{np} demarcate the start and end of precipitation events. Here, in addition, a threshold at $q_c - q_\epsilon$ marks the end of a deep convective episode and the beginning of a stratiform precipitation episode. Subsequently, two outcomes are possible: (i) if $q(t)$ increases to q_c again, then another deep convective episode begins, or (ii) if, instead, $q(t)$ decreases to q_{np} , then the stratiform episode ends and so does the precipitation event. These transitions are illustrated schematically in Figs. 6 and 7.

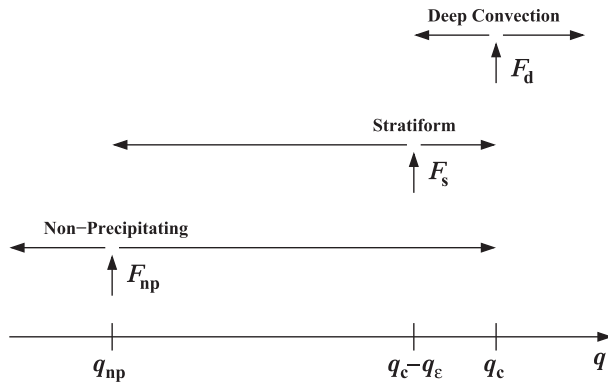


FIG. 6. Range of q values for each state and input q value for each state.

In terms of the dynamics of $q(t)$, the cycle progresses as

$$\begin{aligned} \frac{dq}{dt} &= E_* + D_{np}\dot{\xi} \quad \text{until } q = q_c, \\ \frac{dq}{dt} &= -P_d + D_d\dot{\xi} \quad \text{until } q = q_c - q_e, \\ \frac{dq}{dt} &= -P_s + D_s\dot{\xi} \quad \text{until } q = q_{np} \text{ or } q_c. \end{aligned} \quad (38)$$

If $q = q_{np}$ first, then enter nonprecipitating state.

If $q = q_c$ first, then enter deep convection state.

To keep track of the state of the column, the variables $\sigma_d(t)$ and $\sigma_s(t)$ are assigned values of 0 or 1 accordingly:

$$\begin{aligned} \sigma_d(t) = 0, \sigma_s(t) = 0 & \quad \text{for nonprecipitating state,} \\ \sigma_d(t) = 1, \sigma_s(t) = 0 & \quad \text{for deep convection state,} \\ \sigma_d(t) = 0, \sigma_s(t) = 1 & \quad \text{for stratiform state.} \end{aligned} \quad (39)$$

Notice that knowledge of $q(t)$ alone is not always sufficient to determine whether the column is precipitating or nonprecipitating. This is illustrated in Fig. 6, which shows the σ_d and σ_s values that are possible for each q value. For instance, if $q_{np} < q < q_c - q_e$, the column could be either nonprecipitating or in a stratiform state, and it is the variable $\sigma_s(t)$ that records the memory of these two possibilities. Also notice that a precipitation event is now composed of an alternating sequence of deep convective and stratiform precipitation episodes, where the number of repetitions is random. Figures 8a and 8b show four examples with one deep convective episode within each precipitation event, and it shows one example with two deep convective episodes.

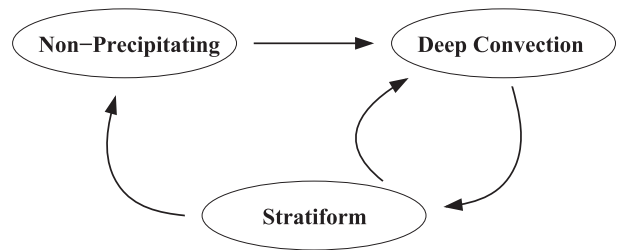


FIG. 7. Transitions between the three states: nonprecipitating, deep convection, and stratiform. Arrows indicate allowed transitions.

The values of the model parameters are listed in Table 2. The rain rates for deep convection, $P_d = 10 \text{ mm h}^{-1}$, and for stratiform, $P_s = 2 \text{ mm h}^{-1}$, are chosen to be somewhat similar to those found in observational analyses (Nesbitt et al. 2006) and distinct from the range already examined in the two-state model. These and other parameters are essentially the same as those used in SN11. Besides the rain-rate parameters P_d and P_s , the other parameters are chosen to match the model CWV pdf and the observed CWV pdf. Such a comparison is easy to carry out using the exact pdf formulas that are presented below. It would be interesting to obtain independent estimates of the parameters based on other observational data or model data.

Before examining the results using the Table 2 parameter choices in the rest of this section, it is useful to briefly consider the limit in which the three-state model reduces to the two-state model and the impacts of the parameter choices on the power-law range. When $P_s = P_d$ and $D_s = D_d$, there is no difference between the dynamics in the stratiform and deep ranges. The model effectively becomes the two-state model with $b = q_c - q_{np}$, and the σ_s , σ_d variables simply track precipitating states with the same parameters. If one starts with parameter values matching those in Table 1, and perturbs the values in small increments, the three-state results evolve smoothly away from those obtained from the two-state model. We do not currently have analytic results for the duration or event-size distributions in the three-state model, but expressions (9)–(12) from the two-state model provide a rough sense of what happens to the power-law range as one moves away from the two-state case. Using the values for P_d and D_d from Table 2 in (10) yields a wet-duration long- t cutoff that is smaller by a factor of 11 than for the parameters of Table 1. Using the values of $q_c - q_{np}$ and D_s for b and D_1 in (9) yields a wet-duration short- t cutoff that is larger by a factor of 64 than the Table 1 case. Thus, the choices of parameters in Table 2, chosen to widen the moisture range over which the stratiform and deep convective

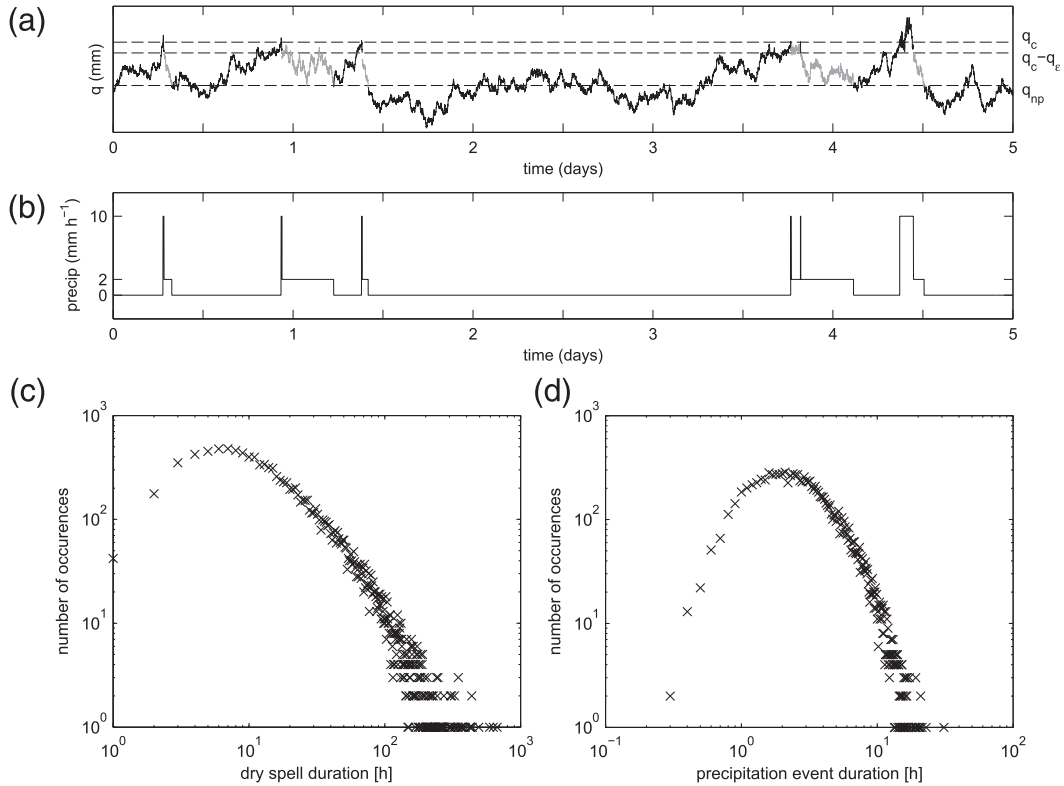


FIG. 8. (top) Sample time series of (a) $q(t)$ and (b) precipitation for the three-state model with deep convective and stratiform precipitation. Dashed lines denote the threshold values q_c , $q_c - q_e$, and q_{np} . Water vapor evolution is shown in black during the nonprecipitating and deep convective episodes and in gray during the stratiform episodes. (bottom) Number of occurrences of (c) dry-spell durations and (d) precipitation event durations for the parameters in Table 2, illustrating a case where the duration cutoff values are not well separated.

states occur, to greatly increase the precipitation rate in the deep convective state, etc., can be anticipated to have the effect of reducing the width of the power-law range for wet durations by almost three orders of magnitude. This is indeed consistent with numerical results for the precipitation event duration seen in Fig. 8d, in which there is effectively no detectable power-law range. Similar considerations suggest that the dry-spell duration short- t cutoff would change by roughly a factor of 16 relative to the Table 1 case but that the long- t cutoff will not change, and this is consistent with numerical results in Fig. 8c.

Note that this three-state model [(35)–(37)] is more similar to the model of SN11 than the two-state model of section 2 is. The reason is that the model of SN11 allowed $P_*(q)$ and $D_1(q)$ to be q dependent with nearly piecewise constant values of two types: an intense (deep convective) and a moderate (stratiform) precipitation state. Here, this same type of behavior is represented by having thresholds at q_c and $q_c - q_e$ for transitions between deep convective and stratiform states.

b. Exact statistics

When precipitation events are partitioned into deep convective and stratiform episodes, it is possible to compute several statistics that quantify the partitioning. In this model, these statistics can be viewed in two ways: (i) as averages that are integrated over all possible CWV values or (ii) as conditional statistics, conditioned on each possible CWV value. In what follows, statistics of

TABLE 2. Parameters for the three-state model with both stratiform and deep convective precipitation.

Symbol	Description	Value
P_d	Deep convective precipitation rate	10 mm h ⁻¹
P_s	Stratiform precipitation rate	2 mm h ⁻¹
E_*	Evaporation rate	0.4 mm h ⁻¹
D_d^2	Forcing variance ($\sigma_d = 1$)	64 mm ² h ⁻¹
D_s^2	Forcing variance ($\sigma_s = 1$)	16 mm ² h ⁻¹
D_{np}^2	Forcing variance ($\sigma_d = \sigma_s = 0$)	8 mm ² h ⁻¹
q_c	Critical CWV	65 mm
$q_c - q_e$	Stratiform threshold CWV	62 mm
q_{np}	Low-threshold CWV	53 mm

these two types are presented in succession. (Derivations are shown mostly in the [appendix](#).)

As a first example of an integrated statistic, one can consider the amount of time spent in each of the three states. This is similar to a “cloud fraction” for each state but computed over time domain without spatial considerations, and only for precipitating cloud. For simplicity, we use cloud fraction for this below (noting that this would not be the same as cloud fraction treated in a climate model radiative code). One obtains

$$\begin{aligned} \text{nonprecipitating fraction} &= P\{\sigma_d = 0, \sigma_s = 0\} \\ &= F_s P_{s \rightarrow \text{np}} \frac{q_c - q_{\text{np}}}{E_{\text{np}}}, \end{aligned} \quad (40)$$

$$\text{deep convection cloud fraction} = P\{\sigma_d = 1\} = F_s \frac{q_\epsilon}{P_d}, \quad (41)$$

$$\begin{aligned} \text{stratiform cloud fraction} &= P\{\sigma_s = 1\} \\ &= F_s P_{s \rightarrow \text{np}} \frac{q_c - q_\epsilon - q_{\text{np}}}{P_s} \\ &\quad - F_s P_{s \rightarrow d} \frac{q_\epsilon}{P_s}, \end{aligned} \quad (42)$$

where F_s enforces the normalization condition that (40)–(42) sum to 1. For the parameters in [Table 2](#), the numerical values are $P\{\sigma_d = 0, \sigma_s = 0\} = 0.89$, $P\{\sigma_d = 1\} = 0.016$, and $P\{\sigma_s = 1\} = 0.098$. From this, one finds that the occurrence fraction of precipitation is $P\{\sigma_d = 1\} + P\{\sigma_s = 1\} = 0.11$; of these occurrences, in turn, the stratiform fraction $P\{\sigma_s = 1\}/(P\{\sigma_d = 1\} + P\{\sigma_s = 1\})$ is 0.86, which is close to the value of 0.84 reported by [Nesbitt et al. \(2006\)](#) for mesoscale convective systems over the ocean.

The quantities $P_{s \rightarrow \text{np}}$ and $P_{s \rightarrow d}$ that enter in (40)–(42) are interesting statistics in and of themselves; they are the probabilities of transition from the stratiform state to either the nonprecipitating state or deep convection state, respectively:

$$P_{s \rightarrow \text{np}} = \frac{1 - \exp[-(2P_s/D_s^2)q_\epsilon]}{1 - \exp[-(2P_s/D_s^2)(q_c - q_{\text{np}})]}, \quad (43)$$

$$P_{s \rightarrow d} = \frac{\exp[-(2P_s/D_s^2)q_\epsilon] - \exp[-(2P_s/D_s^2)(q_c - q_{\text{np}})]}{1 - \exp[-(2P_s/D_s^2)(q_c - q_{\text{np}})]}, \quad (44)$$

which satisfy $P_{s \rightarrow \text{np}} + P_{s \rightarrow d} = 1$. For the parameters in [Table 2](#), the numerical values are $P_{s \rightarrow \text{np}} = 0.56$ and $P_{s \rightarrow d} = 0.44$. The authors are not aware of any estimates of these quantities from observational data.

In addition, the mean precipitation rate and the stratiform rain fraction can be computed from (41) and (42) as

$$\begin{aligned} \langle \text{precip} \rangle &= P_s P\{\sigma_s = 1\} + P_d P\{\sigma_d = 1\} \\ &= F_s P_{s \rightarrow \text{np}} (q_c - q_{\text{np}}) \end{aligned} \quad (45)$$

and

$$\text{stratiform rain fraction} = \frac{P_s P\{\sigma_s = 1\}}{\langle \text{precip} \rangle}. \quad (46)$$

For the parameters in [Table 2](#), the numerical values are $\langle \text{precip} \rangle = 8.5 \text{ mm day}^{-1}$ and stratiform rain fraction of 0.55. The $\langle \text{precip} \rangle$ value is larger than the 5.4 mm day^{-1} recorded during Tropical Ocean and Global Atmosphere Coupled Ocean–Atmosphere Response Experiment (TOGA COARE) ([Short et al. 1997](#)) and the 5.3 mm day^{-1} recorded during the Kwajalein Experiment (KWAJEX; [Yuter et al. 2005](#)), but it is similar to the 9.9 mm day^{-1} measured during a particularly active 2-week period of TOGA COARE ([Short et al. 1997](#)). The stratiform rain fraction of 0.55 is quite close to the 0.56 for the oceanic rainfall from [Nesbitt et al. \(2006\)](#); however, this fraction can vary significantly in nature [see [Schumacher and Houze \(2003\)](#) and references therein].

A common aspect of the statistics (40)–(46) is that they are averages over all possible water vapor values. Specifically, they are related to the integrals

$$P\{\sigma_d = \sigma_s = 0\} = \int_{-\infty}^{q_c} p_{\text{np}}(q) dq, \quad (47)$$

$$P\{\sigma_d = 1\} = \int_{q_c - q_\epsilon}^{\infty} p_d(q) dq, \quad (48)$$

$$P\{\sigma_s = 1\} = \int_{q_{\text{np}}}^{q_c} p_s(q) dq, \quad (49)$$

where $p_{\text{np}}(q)$, $p_d(q)$, and $p_s(q)$ are the q -dependent (stationary) probability densities of the three states. The densities satisfy the overall normalization condition

$$\int [p_{\text{np}}(q) + p_d(q) + p_s(q)] dq = 1. \quad (50)$$

Derivations of (40)–(46) are shown in the [appendix](#).

Explicit formulas for $p_{\text{np}}(q)$, $p_d(q)$, and $p_s(q)$ are derived in the [appendix](#), and they have a piecewise exponential form, as shown in [Fig. 9](#). To facilitate comparison with [Peters and Neelin \(2006\)](#) and [Neelin et al. \(2009\)](#), [Fig. 9](#) also shows the overall pdf of CWV [$p_{\text{np}}(q) + p_d(q) + p_s(q)$] and the pdf of precipitating points [$p_d(q) + p_s(q)$].

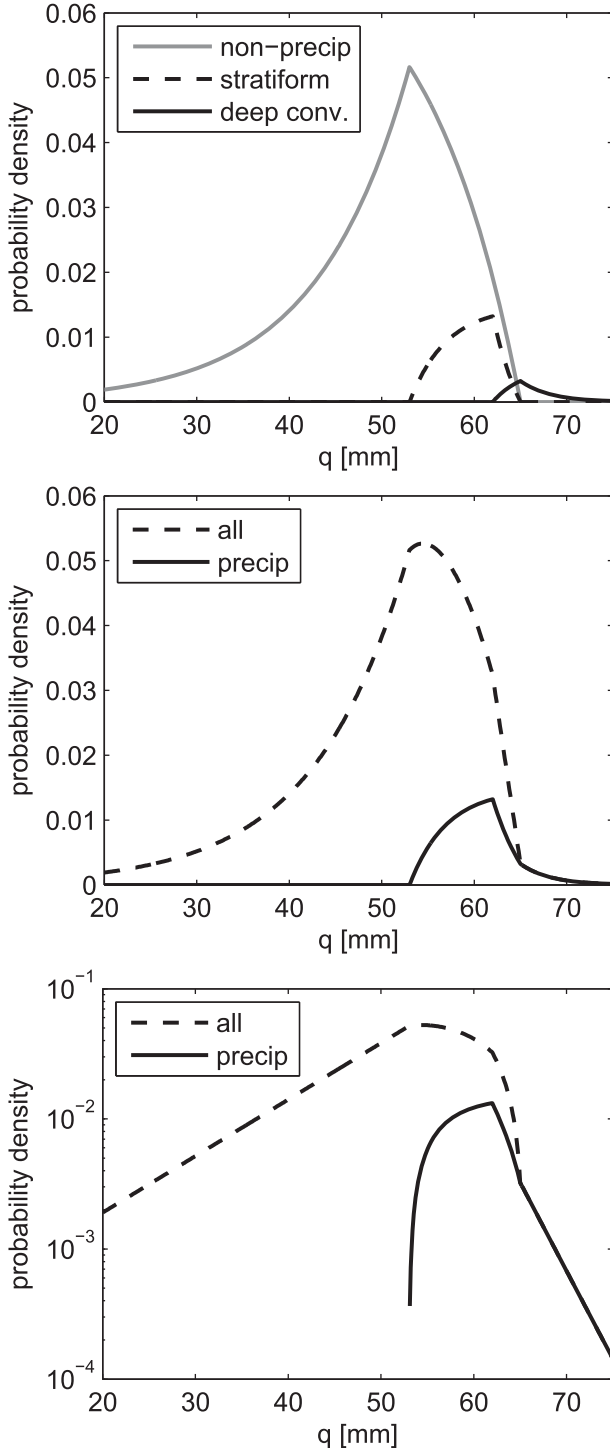


FIG. 9. CWV pdfs for the three-state model. (top) CWV pdfs for the nonprecipitating state (gray), deep convection (solid black), and stratiform (dashed black). (middle) Total pdf of CWV (dashed) and pdf of CWV for the precipitating states (solid). (bottom) As in (middle), except plotted with log-linear axis scaling.

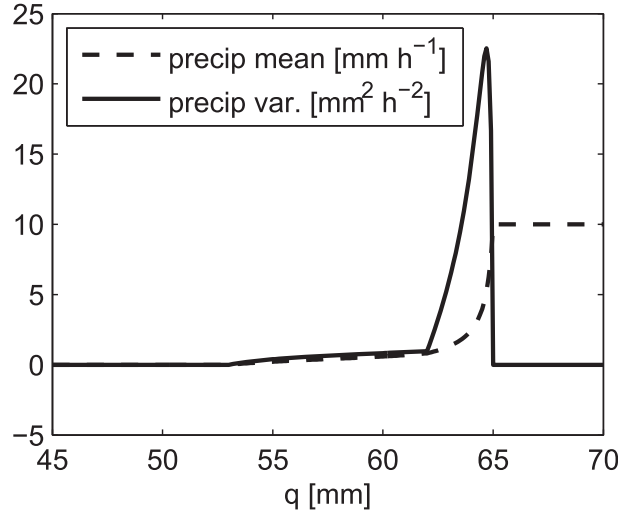


FIG. 10. Precipitation mean (dashed) and variance (solid) for the three-state model with stratiform and deep convective precipitation. Similar considerations for precipitation variance above q_c apply as in Fig. 5.

These latter two pdfs are comparable to those from observational analyses, which are reproduced here in Fig. 1. From these pdfs, one can see that the CWV is typically below $q_c = 65$ mm, even while precipitating, and the pdf has a “long tail” with exponential decay above the critical value. If a stochastic component to the transition threshold were included, there would be a tendency to smooth out these pdfs, similar to the discussion of Fig. 4. If the precipitation rate increased smoothly as a function of q over the stratiform range, this would likewise yield a smoother pdf. The presence of the lower-rain-rate stratiform range (for D_s as specified in Table 2) does produce an increase in the pdf for precipitating points just below q_c .

While (45) described the mean precipitation integrated over all possible q values, analogous statistics can be found for particular q values. The mean and second moment of precipitation, conditioned on column water vapor value q , are

$$\langle \text{precip} \rangle(q) = \frac{P_s p_s(q) + P_d p_d(q)}{P_{np}(q) + p_s(q) + p_d(q)}, \quad (51)$$

$$\langle \text{precip}^2 \rangle(q) = \frac{P_s^2 p_s(q) + P_d^2 p_d(q)}{P_{np}(q) + p_s(q) + p_d(q)}. \quad (52)$$

Figure 10 shows plots of the mean and the variance, $\langle \text{precip}^2 \rangle(q) - \langle \text{precip} \rangle^2(q)$. The form has the same qualitative features as in the observational analysis of Peters and Neelin (2006) and Neelin et al. (2009), as reproduced here in Fig. 1: q_c marks a rapid transition in the mean precipitation and a peak in precipitation variance.

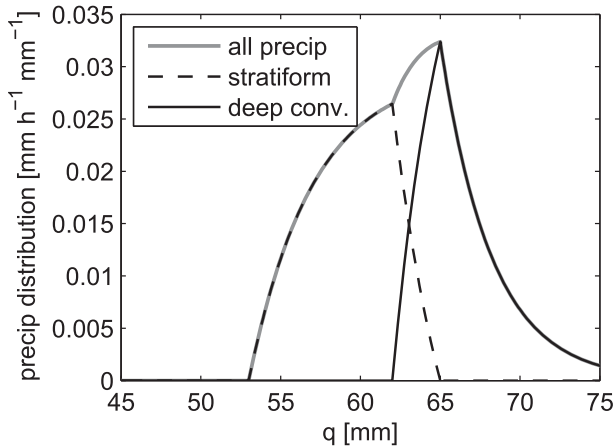


FIG. 11. Precipitation distribution functions for the total (gray), deep convective (solid black), and stratiform (dashed black).

Furthermore, the contributions to the mean precipitation [see (45)] can be displayed for each CWV: How much rain falls at a given CWV value q ? This quantity could perhaps be called a “precipitation distribution function”:

$$\text{precipitation distribution} = P_s p_s(q) + P_d p_d(q). \quad (53)$$

Figure 11 plots this distribution along with its partitioning into stratiform and deep convective components:

$$\text{stratiform precipitation distribution} = P_s p_s(q), \quad (54)$$

$$\text{deep convective precipitation distribution} = P_d p_d(q). \quad (55)$$

The total distribution has a similar shape to that seen in observational analyses in Fig. 6 of Neelin et al. (2009): large portions of precipitation fall both below and above q_c . Furthermore, through the breakdown of the total into its two components, one sees that while, by construction, deep convection is responsible for the rainfall above q_c , stratiform precipitation yields a reasonable representation for the rainfall below q_c . In SN11, a similar hysteresis was represented by a Markov jump process with a probability for precipitation termination below q_c . Here, the identification with stratiform precipitation is physically appealing, and the results suggest that a simple deterministic transition rule, with stratiform precipitation occurring on the downward transition from the convective state, can capture features of the observed pdf near the critical point. It also suggests that observational analysis to break out stratiform versus deep convective precipitation in similar conditional pdfs will be useful to distinguish among these processes.

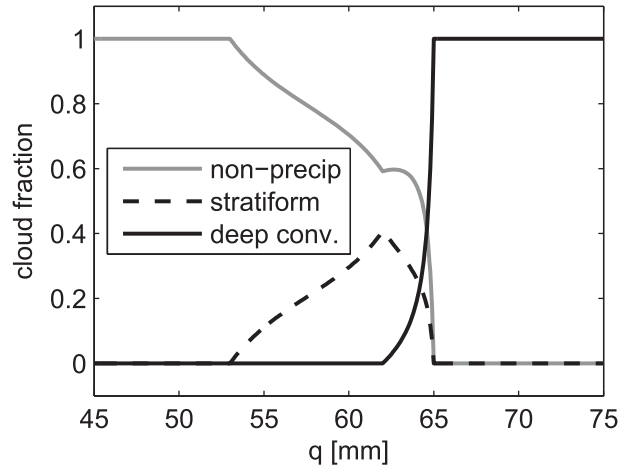


FIG. 12. Cloud fractions (from temporal statistics), conditioned on each CWV value q , for the nonprecipitating state (gray), deep convection (solid black), and stratiform (dashed black).

Last, while cloud fractions were given in (40)–(42) as integrations over all possible q values, analogous statistics can be found for particular q values. Specifically, given a CWV value of q , the cloud fraction can be computed as

$$\begin{aligned} &\text{conditional nonprecipitating fraction} \\ &= \frac{P_{\text{np}}(q)}{P_{\text{np}}(q) + P_s(q) + P_d(q)}, \end{aligned} \quad (56)$$

$$\begin{aligned} &\text{conditional deep convective cloud fraction} \\ &= \frac{P_d(q)}{P_{\text{np}}(q) + P_s(q) + P_d(q)}, \end{aligned} \quad (57)$$

$$\begin{aligned} &\text{conditional stratiform cloud fraction} \\ &= \frac{P_s(q)}{P_{\text{np}}(q) + P_s(q) + P_d(q)}. \end{aligned} \quad (58)$$

As shown in Fig. 12, the conditional cloud fractions have a rapid transition at q_c . Above q_c , only the deep convective state occurs. Below q_c , the cloud fractions progress from only nonprecipitating to a mixture of nonprecipitating and stratiform as CWV increases toward q_c . At its peak, the conditional stratiform cloud fraction is roughly 0.4 when CWV is just below q_c .

To summarize, two types of statistics were presented: those that encompass precipitation properties (i) integrated over all possible CWV values or (ii) isolated at each CWV value independently. The former could be connected with traditional observational analyses, and the latter are in line with new ways to analyze observational data. In particular, many of the statistics fit

within the theme of the “transition to strong convection” (Neelin et al. 2009), and they also suggest, in addition to considering the temporal onset associated with convective conditional instability, the importance of also considering the reverse transition from strong convection to stratiform precipitation upon moving downward across the critical point.

6. Discussion

a. Additional statistics

In addition to the statistics presented here, further statistics could also be computed analytically. Examples include the event-size distribution for the three-state model, the stratiform event-size distribution, and autocorrelation functions. These statistics can be found analytically using Laplace transforms, and they will be presented elsewhere in the future.

b. Relation to renewal processes

As stated in section 1, the prototype models have the form of renewal processes (Cox 1962). In such a process, a state variable [here $\sigma(t)$ or $\sigma_d(t)$ and $\sigma_s(t)$] makes random transitions between states. The time intervals between state transitions are determined by the event-duration pdfs, which are $p_{r0}(t)$ and $p_{r1}(t)$ here for the two-state model. In many precipitation models that can be found in the literature, the form of these pdfs is assigned empirically based on observed data for precipitation alone. Here, in contrast, the form of $p_{r0}(t)$ and $p_{r1}(t)$ arises from joint precipitation–water vapor dynamics. In other words, it is the water vapor dynamics, interacting with a threshold, that is fundamental in the prototype models here. The characterization as a renewal process is secondary, and it applies only to the precipitation indicator $\sigma(t)$, not to the detailed water vapor dynamics of $q(t)$. Nevertheless, this characterization as a renewal process can be useful for computing marginal statistics of precipitation that do not rely on the detailed evolution of the CWV; examples include the precipitation-event-size distribution, the precipitation autocorrelation function, etc.

c. Relation to ISCCP cloud regimes obtained from cluster algorithms

It is tempting to compare the present paper’s model statistics to empirically defined cloud regime data, such as that defined from a cluster analysis of data from the International Satellite Cloud Climatology Project (ISCCP) (Jakob and Tselioudis 2003; Rossow et al. 2005; Jakob and Schumacher 2008). However, that cloud regime analysis was based on data with a relatively large

footprint of $O(280)$ km, whereas the present model was aimed at analyses of data with a smaller footprint of $O(20)$ km (Peters and Neelin 2006; Neelin et al. 2009). In the future, perhaps this scale gap could be closed somehow to allow a meaningful comparison.

d. Implications for convective parameterizations in GCMs

One interesting feature of the prototype models is the element of hysteresis: after water vapor crosses above q_c , the precipitation event does not end when water vapor returns to q_c ; instead, CWV must fall to a second, lower threshold q_{np} in order for precipitation to end. This dynamics with two distinct thresholds—one for onset and one for shutdown—is different from the triggers used in many GCM convective parameterizations. In many GCMs, a single threshold is used for both onset and shutdown. The prototype models here offer simple ways to include the hysteresis and multiple-threshold behavior of convection.

A second interesting feature of the prototypes is the important role of stratiform precipitation. In the two-state model, with no distinction between deep convective and stratiform precipitation, the CWV pdf gives only a qualitative sketch of the observed features. For instance, the maximum in Fig. 4 for precipitating points occurs at the critical value rather than below. In the three-state model, by partitioning deep convective and stratiform precipitation, the realism of the statistics is improved.

Based on these results, one would expect GCM convective parameterizations to benefit from including a stratiform component. Indeed, several studies have demonstrated such benefits (Moncrieff and Liu 2006; Khouider and Majda 2006; Khouider et al. 2011; Frenkel et al. 2013), including a case with a stochastic parameterization (Biello et al. 2010; Frenkel et al. 2013). The present prototypes offer simple ways to parameterize a stratiform component. In particular, implementing two or three thresholds—instead of just one—appears to accomplish some aspects of this; and the stochastic thresholds of Stechmann and Neelin (2011) offer another simple alternative.

7. Conclusions

Two prototype models were presented for precipitation and water vapor evolution. Among the goals, a major aim was to understand the processes underlying the joint statistics of precipitation and water vapor. To this end, in the first prototype, a two-state model involved a precipitating state and a nonprecipitating state as a minimal representation of convective onset and

shutdown. In the other prototype, a three-state model was introduced to partition precipitation events into deep convective and stratiform episodes. Both prototype models are exactly solvable for many quantities, and analytical formulas were presented for model statistics. The tails of pdfs and the statistics of extreme events can thus be described unambiguously, free from statistical sampling errors, and insight can be obtained into the governing physics.

As the simplest prototype, the two-state model was seen to be sufficient for several basic features, including in particular the precipitation-event-size distribution p_S . A prominent feature of p_S was a range of power-law scaling with exponent $-3/2$. This scaling was valid in between a characteristic small-event-size cutoff, $b^2 P_*/D_1^2$, and a characteristic large-event-size cutoff, D_1^2/P_* . This ratio D_1^2/P_* is also the characteristic scale of the exponential decay of the CWV pdf. This provides a useful prototype for understanding several features of event-size distributions seen in observations. Among the most interesting are associated with the demonstration that stochastic forcing by variations in moisture convergence driving moisture across a threshold for the onset of rainfall is sufficient to set up a power-law range with an exponent roughly similar to observational estimates. The key ingredients are the threshold, the memory provided by the prognostic equation for water vapor (or total water if condensate is included), and the drift toward the threshold from both sides (by evaporation from below and by precipitation from above, each potentially modified by mean moisture convergence).

This interpretation is consistent with prior discussion (Peters et al. 2001; Peters and Neelin 2006) in terms of self-organized criticality; the system is forced toward the critical point from below, followed by an internal dissipation mechanism that returns the system toward the threshold from above. Indeed, first-passage processes are among the simplest prototypes for self-organized criticality (Redner 2001). Aspects gained here are (i) the direct relationship to equations simplified from meteorological models, (ii) a clear prototype for how the time-domain interactions give the power-law ranges in precipitation event and dry-spell distributions and the cutoffs for these ranges, and (iii) an understanding of the relationship between the long tails above the critical point and the distributions with power-law ranges. Regarding (ii), in seeking prototype behavior for power-law ranges, one might be tempted to conjecture that neighbor interactions in the spatial domain could be essential to establishing the set of properties near critical. While these might play a role in spatial clustering properties, the present model

suggests that simple time-domain interactions involving the onset threshold are the leading effect in establishing the power-law range and in setting the difference in cutoff values in event size or dry-event-duration distributions. Regarding (iii), in typical prototype models for self-organized criticality, as well as in standard assumptions for convective quasi equilibrium, the system is tightly confined just below critical [for a review, see Neelin et al. (2008)] so the long tails observed for the distribution of precipitating points above critical would appear puzzling. In the two-state model, these long tails and the large-event-size cutoff arise naturally together: both are governed by the same scale and both depend on the fluctuations of moisture convergence being sufficiently large compared to the loss rate by precipitation. The power-law range for the dry-event durations arises by the flipside of this dynamics, with the long-duration cutoff given by moisture convergence fluctuations versus slow evaporative driving.

For precipitating-point water vapor distributions, the two-state model gives results in which one can recognize key features of the observations but in highly simplified form. Without including all the processes used to reproduce these distributions in SN11, such as onset probabilities, a three-state model is a natural next-most-simple model and proves able to better capture a number of these features. The three-state model provides formulas for the partitioning of precipitation into deep convective and stratiform components, the latter simply having a lower rain rate and an onset dictated by downward transition from the deep convective state. In addition to traditional statistics such as mean precipitation and stratiform cloud fraction, more detailed versions were shown where, for instance, the contributions to total precipitation could be broken down for each possible water vapor value q . This latter type of statistic is in the spirit of the observational analyses of Bretherton et al. (2002) and later Peters and Neelin (2006) and Neelin et al. (2009), who identified a critical value q_c of water vapor that marks the transition to strong convection. This provides a prototype for the transition between strong convection and stratiform precipitation near q_c that suggests many aspects of this can be captured in a simple time-domain formulation that may be useful for parameterization.

Acknowledgments. The research of S.N.S. is partially supported by the ONR Young Investigator Program through Grant ONR N00014-12-1-0744, and J.D.N. is partially supported by National Science Foundation Grant AGS-1102838 and NOAA Grant NA11OAR4310099. The authors thank A. Corral and T. Schneider for helpful discussion.

APPENDIX A

Derivations for Two-State Model for Convective Onset

a. Precipitation events

At the start of the precipitation event, the water vapor is at its critical value $q = q_c$, and the event ends when the water vapor has decreased to $q = q_{np}$. In this situation, the pdf $p_1(q, t)$ for the water vapor evolves according to a Fokker–Planck equation:

$$\partial_t p_1 - P_* \partial_q p_1 = \frac{D_1^2}{2} \partial_q^2 p_1, \tag{A1}$$

$$p_1(q_{np}, t) = 0, \tag{A2}$$

$$p_1(q, 0) = \delta(q - q_c), \tag{A3}$$

where the PDE is satisfied on $q_{np} < q < \infty$ with an absorbing boundary at $q = q_{np}$. The solution is

$$p_1(q, t) = \frac{1}{\sqrt{2\pi D_1^2 t}} \left\{ \exp \left[-\frac{(q - q_c + P_* t)^2}{2D_1^2 t} \right] - \exp \left(\frac{2P_* b}{D_1^2} \right) \exp \left[-\frac{(q - q_{np} + b + P_* t)^2}{2D_1^2 t} \right] \right\} \tag{A4}$$

(see Redner 2001). Since an event ends when the water vapor reaches the threshold $q = q_{np}$, the pdf $p_{t1}(t)$ of the event duration is equivalent to the probability flux at the threshold:

$$p_{t1}(t) = \left(P_* p_1 + \frac{D_1^2}{2} \frac{\partial p_1}{\partial q} \right) \Big|_{q=q_{np}} = \frac{D_1^2}{2} \frac{\partial p_1}{\partial q} \Big|_{q=q_{np}}, \tag{A5}$$

which is given explicitly in (5).

b. Dry spells

At the start of a dry spell, the water vapor is at the low threshold value $q = q_{np}$, and the dry spell ends when the water vapor has increased to $q = q_c$. In this situation, the pdf $p_0(q, t)$ for the water vapor evolves according to a Fokker–Planck equation:

$$\partial_t p_0 + E_* \partial_q p_0 = \frac{D_0^2}{2} \partial_q^2 p_0, \tag{A6}$$

$$p_0(q_c, t) = 0, \tag{A7}$$

$$p_0(q, 0) = \delta(q - q_{np}), \tag{A8}$$

where the PDE is satisfied on $-\infty < q < q_c$ with an absorbing boundary at $q = q_c$. The solution is found similarly to the wet-spell case but with some changes in parameters.

c. Cloud fractions and stationary pdf

The equilibrium cloud fraction is defined in terms of the probability densities $p_0(q)$ and $p_1(q)$ for the dry and wet states at each CWV value q . In equilibrium, the functions p_0 and p_1 satisfy the following system of Fokker–Planck equations:

$$E_* \partial_q p_0 = \frac{D_0^2}{2} \partial_q^2 p_0 - \delta(q - q_{np}) f_1 \Big|_{q=q_{np}}, \quad -\infty < q < q_c, \tag{A9}$$

$$-P_* \partial_q p_1 = \frac{D_1^2}{2} \partial_q^2 p_1 + \delta(q - q_c) f_0 \Big|_{q=q_c}, \quad q_{np} < q < \infty, \tag{A10}$$

with absorbing boundary conditions

$$p_0(q_c) = 0, \tag{A11}$$

$$p_1(q_{np}) = 0, \tag{A12}$$

and where f_0 and f_1 are the probability fluxes

$$f_0 = E_* p_0 - \frac{D_0^2}{2} \partial_q p_0, \tag{A13}$$

$$f_1 = -P_* p_1 - \frac{D_1^2}{2} \partial_q p_1. \tag{A14}$$

The Dirac delta source terms in (A9) and (A10) represent transitions between the precipitating and non-precipitating states at the absorbing boundaries, $q = q_c$ and $q = q_{np}$. Because of these Dirac delta source terms, two types of consistency conditions arise. First, the consistency condition

$$f_0 \Big|_{q=q_c} = -f_1 \Big|_{q=q_{np}} \tag{A15}$$

or equivalently

$$-\frac{D_0^2}{2} \partial_q p_0 \Big|_{q=q_c} = \frac{D_1^2}{2} \partial_q p_1 \Big|_{q=q_{np}} \tag{A16}$$

arises as a balance in the fluxes. This condition arises from integrating (A9) and (A10) over their domains of validity and assuming that $p_0 \rightarrow 0$ and $\partial_q p_0 \rightarrow 0$ as $q \rightarrow -\infty$ and that $p_1 \rightarrow 0$ and $\partial_q p_1 \rightarrow 0$ as $q \rightarrow \infty$. The same condition arises from both (A9) and (A10) for this two-state system, and it represents an integrated balance in the fluxes: the flux out of the dry state must be balanced

by a flux into the wet state and vice versa. Second, the Dirac delta sources cause local jumps in the fluxes. The jumps satisfy the consistency conditions

$$f_0|_{q=q_{\text{np}}^+} - f_0|_{q=q_{\text{np}}^-} = -f_1|_{q=q_{\text{np}}}, \quad (\text{A17})$$

$$f_1|_{q=q_c^+} - f_1|_{q=q_c^-} = f_0|_{q=q_c}. \quad (\text{A18})$$

These conditions arise from integrating (A9) over the small interval $q_{\text{np}} - \lambda < q < q_{\text{np}} + \lambda$ and integrating (A10) over the small interval $q_c - \lambda < q < q_c + \lambda$ and taking the limit as $\lambda \rightarrow 0$. As opposed to the integrated flux balance in (A15), the conditions (A17) and (A18) are local balances, at particular CWV values, between an input flux and a jump in flux. Because of these jumps, the functions $p_0(q)$ and $p_1(q)$ will be continuous but will have jumps in their derivatives.

To solve for the stationary solution, one can first integrate (A9) and (A10) over each of the intervals $-\infty < q < q_{\text{np}}$, $q_{\text{np}} < q < q_c$, and $q_c < q < \infty$. Within each of these intervals, the Dirac delta terms are zero, the equations are uncoupled, and $p_0(q)$ and $p_1(q)$ are exponential. Several integration constants arise, and their values are determined by the following constraints: decay of $p_0(q)$ and $p_1(q)$ and their derivatives as q tends toward $\pm\infty$, the boundary conditions (A11) and (A12), continuity of $p_0(q)$ at $q = q_{\text{np}}$ and $p_1(q)$ at $q = q_c$, the jump conditions in (A17) and (A18), the integrated flux balance conditions in (A15), and the overall normalization condition in (23). In the end, the stationary solution to (A9)–(A18) is piecewise exponential as written explicitly in (24)–(27) and shown in Fig. 4.

APPENDIX B

Derivations for Three-State Model with Stratiform Precipitation

a. Stratiform events

Precipitation events now include both deep convective and stratiform rain, and they follow an alternating sequence of events of the form deep–stratiform or deep–stratiform–deep–stratiform or deep–stratiform–deep–stratiform–deep–stratiform, etc. The deep convective portions are determined in a similar way as in appendix A, whereas the stratiform portions are considered next.

For a stratiform episode, CWV is initially at $q = q_c - q_\epsilon$, and the episode ends when CWV either decreases to q_{np} or increases to q_c . This evolution is described by the following Fokker–Planck equation with two absorbing boundaries:

$$\partial_t p_s - P_s \partial_q p_s = \frac{D_s^2}{2} \partial_q^2 p_s, \quad (\text{B1})$$

$$p_s(q_{\text{np}}, t) = 0, \quad (\text{B2})$$

$$p_s(q_c, t) = 0, \quad (\text{B3})$$

$$p_s(q, 0) = \delta(q - q_c + q_\epsilon), \quad (\text{B4})$$

where the PDE is satisfied on $q_{\text{np}} < q < q_c$ with absorbing boundaries at $q = q_{\text{np}}$ and $q = q_c$. At the start of the stratiform event, the water vapor is at the value $q = q_c - q_\epsilon$, which is the threshold for the end of a deep convective episode.

Two quantities are of interest here: $P_{s \rightarrow \text{np}}$ and $P_{s \rightarrow d}$. These are the transition probabilities from the stratiform state to the nonprecipitating and deep convective states, respectively. In terms of the problem in (B1)–(B4), $P_{s \rightarrow \text{np}}$ is the probability of first reaching the point q_{np} , and $P_{s \rightarrow d}$ is the probability of first reaching the point q_c . This problem of first exit from an interval has well-known solutions (Redner 2001; Gardiner 2004) that are written explicitly in (43) and (44).

b. Cloud fractions and stationary pdf

The equilibrium cloud fractions are defined in terms of the probability densities $p_{\text{np}}(q)$, $p_d(q)$, and $p_s(q)$ for the nonprecipitating, deep convective, and stratiform states at each CWV value q . In equilibrium, the functions p_{np} , p_d , and p_s satisfy the following system of Fokker–Planck equations:

$$E_* \partial_q p_{\text{np}} = \frac{D_{\text{np}}^2}{2} \partial_q^2 p_{\text{np}} - \delta(q - q_{\text{np}}) f_s|_{q=q_{\text{np}}} \quad \text{for} \\ -\infty < q < q_c, \quad (\text{B5})$$

$$-P_d \partial_q p_d = \frac{D_d^2}{2} \partial_q^2 p_d + \delta(q - q_c) (f_{\text{np}}|_{q=q_c} + f_s|_{q=q_c}) \quad \text{for} \\ q_c - q_\epsilon < q < \infty, \quad (\text{B6})$$

$$-P_s \partial_q p_s = \frac{D_s^2}{2} \partial_q^2 p_s - \delta(q - q_c + q_\epsilon) f_d|_{q=q_c - q_\epsilon} \quad \text{for} \\ q_{\text{np}} < q < q_c; \quad (\text{B7})$$

with absorbing boundary conditions

$$p_{\text{np}}(q_c) = 0, \quad (\text{B8})$$

$$p_d(q_c - q_\epsilon) = 0, \quad (\text{B9})$$

$$p_s(q_c) = p_s(q_{\text{np}}) = 0; \quad (\text{B10})$$

and where f_{np}, f_d, f_s are the probability fluxes

$$f_{np} = E_* p_{np} - \frac{D_{np}^2}{2} \partial_q p_{np}, \tag{B11}$$

$$f_d = -P_d p_d - \frac{D_d^2}{2} \partial_q p_d, \tag{B12}$$

$$f_s = -P_s p_s - \frac{D_s^2}{2} \partial_q p_s. \tag{B13}$$

The Dirac delta source terms in (B5)–(B7) represent transitions between the states at their absorbing boundaries. Because of these Dirac delta source terms, two types of consistency conditions arise. First, the consistency conditions

$$f_{np}|_{q=q_c} = -f_s|_{q=q_{np}}, \tag{B14}$$

$$-f_d|_{q=q_c - q_\epsilon} = f_{np}|_{q=q_c} + f_s|_{q=q_c}, \tag{B15}$$

$$f_s|_{q=q_c} - f_s|_{q=q_{np}} = -f_d|_{q=q_c - q_\epsilon} \tag{B16}$$

arise as balances in the fluxes. These conditions arise from integrating (B5)–(B7) over their domains of validity and assuming appropriate decay conditions as $q \rightarrow \pm\infty$. In essence, (B14)–(B16) represent integrated balance conditions for fluxes into and out of each of the three states. Second, the Dirac delta sources cause local jumps in the fluxes. The jumps satisfy the consistency conditions

$$f_{np}|_{q=q_{np}^+} - f_{np}|_{q=q_{np}^-} = -f_s|_{q=q_{np}}, \tag{B17}$$

$$f_d|_{q=q_c^+} - f_d|_{q=q_c^-} = f_{np}|_{q=q_c} + f_s|_{q=q_c}, \tag{B18}$$

$$f_s|_{q=(q_c - q_\epsilon)^+} - f_s|_{q=(q_c - q_\epsilon)^-} = -f_d|_{q=q_c - q_\epsilon}. \tag{B19}$$

These conditions arise from integrating (B5)–(B7) over small intervals centered on the points q_{np}, q_c , and $q_c - q_\epsilon$, respectively. For instance, (B17) is found by integrating (B5) over the small interval $q_{np} - \lambda < q < q_{np} + \lambda$ and taking the limit as $\lambda \rightarrow 0$. As opposed to the integrated flux balances in (B14)–(B16), the conditions (B17)–(B19) are local balances, at particular CWV values, between an input flux and a jump in a flux. Because of these jumps, the functions $p_{np}(q), p_d(q)$, and $p_s(q)$ will be continuous but will have jumps in their derivatives.

To solve for the stationary solution, one can first integrate (B5)–(B7) over each of the four intervals $-\infty < q < q_{np}, q_{np} < q < q_c - q_\epsilon, q_c - q_\epsilon < q < q_c$, and $q_c < q < \infty$. Within each of these intervals, the Dirac delta terms are zero, the equations are uncoupled, and the functions $p_{np}(q), p_d(q)$, and $p_s(q)$ are exponential. Several integration constants arise, and their values are determined by the following constraints: decay of $p_{np}(q), p_d(q)$, and $p_s(q)$ and their derivatives as q tends toward $\pm\infty$; the boundary conditions (B8)–(B10); continuity of $p_{np}(q)$ at $q = q_{np}, p_d(q)$ at $q = q_c$, and $p_s(q)$ at $q = q_c - q_\epsilon$; the jump conditions in (B17)–(B19); the integrated flux balance conditions in (B14)–(B16); and the overall normalization condition in (50). In the end, the stationary solution to (B5)–(B19) is piecewise exponential:

$$p_{np}(q) = \frac{F_{np}}{E_{np}} \left\{ 1 - \exp \left[-\frac{2E_{np}}{D_{np}^2} (q_c - q_{np}) \right] \right\} \exp \left[\frac{2E_{np}}{D_{np}^2} (q - q_{np}) \right] \quad \text{for } q < q_{np}, \tag{B20}$$

$$p_{np}(q) = \frac{F_{np}}{E_{np}} \left\{ 1 - \exp \left[\frac{2E_{np}}{D_{np}^2} (q - q_c) \right] \right\} \quad \text{for } q_{np} < q < q_c, \tag{B21}$$

$$p_d(q) = \frac{F_d}{P_d} \left\{ 1 - \exp \left[-\frac{2P_d}{D_d^2} (q - q_c + q_\epsilon) \right] \right\} \quad \text{for } q_c - q_\epsilon < q < q_c, \tag{B22}$$

$$p_d(q) = \frac{F_d}{P_d} \left\{ 1 - \exp \left[-\frac{2P_d}{D_d^2} q_\epsilon \right] \right\} \exp \left[-\frac{2P_d}{D_d^2} (q - q_c) \right] \quad \text{for } q_c < q, \tag{B23}$$

$$p_s(q) = \frac{F_s}{P_s} P_{s \rightarrow np} \left\{ 1 - \exp \left[-\frac{2P_s}{D_s^2} (q - q_{np}) \right] \right\} \quad \text{for } q_{np} < q < q_c - q_\epsilon, \tag{B24}$$

$$p_s(q) = \frac{F_s}{P_s} P_{s \rightarrow d} \left\{ \exp \left[-\frac{2P_s}{D_s^2} (q - q_c) \right] - 1 \right\} \quad \text{for } q_c - q_\epsilon < q < q_c. \quad (\text{B25})$$

These functions are also plotted in Fig. 9. The quantities $P_{s \rightarrow \text{np}}$ and $P_{s \rightarrow d}$ are the transition probabilities given in (43) and (44). The quantities F_{np} , F_d , and F_s are the input fluxes into the nonprecipitating, deep convective, and stratiform states, respectively. They are defined by the right-hand sides of (B14)–(B16), respectively, and illustrated schematically in Fig. 6. Their explicit values are

$$F_{\text{np}} = F_s P_{s \rightarrow \text{np}}, \quad (\text{B26})$$

$$F_d = F_s, \quad (\text{B27})$$

$$F_s = \left(P_{s \rightarrow \text{np}} \frac{q_c - q_{\text{np}}}{E_{\text{np}}} + \frac{q_\epsilon}{P_d} + P_{s \rightarrow \text{np}} \frac{q_c - q_\epsilon - q_{\text{np}}}{P_s} - P_{s \rightarrow d} \frac{q_\epsilon}{P_s} \right)^{-1}, \quad (\text{B28})$$

where F_s also arises as the normalization constant for the cloud fractions in (40)–(42).

REFERENCES

- Andrade, R. F. S., H. J. Schellnhuber, and M. Claussen, 1998: Analysis of rainfall records: Possible relation to self-organized criticality. *Physica A*, **254** (3–4), 557–568, doi:10.1016/S0378-4371(98)00057-0.
- Arakawa, A., and W. H. Schubert, 1974: Interaction of a cumulus cloud ensemble with the large-scale environment, Part I. *J. Atmos. Sci.*, **31**, 674–701, doi:10.1175/1520-0469(1974)031<0674:IOACCE>2.0.CO;2.
- Bernardara, P., C. De Michele, and R. Rosso, 2007: A simple model of rain in time: An alternating renewal process of wet and dry states with a fractional (non-Gaussian) rain intensity. *Atmos. Res.*, **84**, 291–301, doi:10.1016/j.atmosres.2006.09.001.
- Betts, A. K., 1986: A new convective adjustment scheme. Part I: Observational and theoretical basis. *Quart. J. Roy. Meteor. Soc.*, **112**, 677–692.
- Biello J. A., B. Khouider, and A. J. Majda, 2010: A stochastic multicloud model for tropical convection. *Commun. Math. Sci.*, **8**, 187–216, doi:10.4310/CMS.2010.v8.n1.a10.
- Bretherton, C. S., M. E. Peters, and L. E. Back, 2002: Relationships between water vapor path and precipitation over the tropical oceans. *J. Climate*, **15**, 2907–2920, doi:10.1175/1520-0442(2002)015<2907:ASMOAC>2.0.CO;2.
- Cheng, C.-P., and R. A. Houze Jr., 1979: The distribution of convective and mesoscale precipitation in GATE radar echo patterns. *Mon. Wea. Rev.*, **107**, 1370–1381, doi:10.1175/1520-0493(1979)107<1370:TDOCAM>2.0.CO;2.
- Christensen, K., and N. R. Moloney, 2005: *Complexity and Criticality*. Imperial College Press, 392 pp.
- Cox, D. R., 1962: *Renewal Theory*. Methuen, 142 pp.
- Foufoula-Georgiou, E., and D. P. Lettenmaier, 1987: A Markov renewal model for rainfall occurrences. *Water Resour. Res.*, **23**, 875–884, doi:10.1029/WR023i005p00875.
- Frenkel, Y., A. J. Majda, and B. Khouider, 2013: Stochastic and deterministic multicloud parameterizations for tropical convection. *Climate Dyn.*, **41**, 1527–1551, doi:10.1007/s00382-013-1678-z.
- Galewsky, J., A. Sobel, and I. Held, 2005: Diagnosis of subtropical humidity dynamics using tracers of last saturation. *J. Atmos. Sci.*, **62**, 3353–3367, doi:10.1175/JAS3533.1.
- Gardiner, C. W., 2004: *Handbook of Stochastic Methods: For Physics, Chemistry, and the Natural Sciences*. Springer Series in Synergetics, Vol. 13, Springer-Verlag, 442 pp.
- Green, J. R., 1964: A model for rainfall occurrence. *J. Roy. Stat. Soc.*, **26B**, 345–353.
- Hilburn, K. A., and F. J. Wentz, 2008: Intercalibrated passive microwave rain products from the unified microwave ocean retrieval algorithm (UMORA). *J. Appl. Meteor. Climatol.*, **47**, 778–794, doi:10.1175/2007JAMC1635.1.
- Holloway, C. E., and J. D. Neelin, 2009: Moisture vertical structure, column water vapor, and tropical deep convection. *J. Atmos. Sci.*, **66**, 1665–1683, doi:10.1175/2008JAS2806.1.
- Houze, R. A., Jr., 1989: Observed structure of mesoscale convective systems and implications for large-scale heating. *Quart. J. Roy. Meteor. Soc.*, **115**, 425–461, doi:10.1002/qj.49711548702.
- Jakob, C., and G. Tselioudis, 2003: Objective identification of cloud regimes in the tropical western Pacific. *Geophys. Res. Lett.*, **30**, 2082, doi:10.1029/2003GL018367.
- , and C. Schumacher, 2008: Precipitation and latent heating characteristics of the major tropical western Pacific cloud regimes. *J. Climate*, **21**, 4348–4364, doi:10.1175/2008JCL12122.1.
- Khouider, B., and A. J. Majda, 2006: A simple multicloud parameterization for convectively coupled tropical waves. Part I: Linear analysis. *J. Atmos. Sci.*, **63**, 1308–1323, doi:10.1175/JAS3677.1.
- , and —, 2008: Equatorial convectively coupled waves in a simple multicloud model. *J. Atmos. Sci.*, **65**, 3376–3397, doi:10.1175/2008JAS2752.1.
- , A. St-Cyr, A. J. Majda, and J. Tribbia, 2011: The MJO and convectively coupled waves in a coarse-resolution GCM with a simple multicloud parameterization. *J. Atmos. Sci.*, **68**, 240–264, doi:10.1175/2010JAS3443.1.
- Majda, A. J., and B. Khouider, 2002: Stochastic and mesoscopic models for tropical convection. *Proc. Natl. Acad. Sci. USA*, **99**, 1123–1128, doi:10.1073/pnas.032663199.
- , and S. N. Stechmann, 2008: Stochastic models for convective momentum transport. *Proc. Natl. Acad. Sci. USA*, **105**, 17 614–17 619, doi:10.1073/pnas.0806838105.
- , and —, 2009: A simple dynamical model with features of convective momentum transport. *J. Atmos. Sci.*, **66**, 373–392, doi:10.1175/2008JAS2805.1.
- Mapes, B. E., 1993: Gregarious tropical convection. *J. Atmos. Sci.*, **50**, 2026–2037, doi:10.1175/1520-0469(1993)050<2026:GTC>2.0.CO;2.
- , 2000: Convective inhibition, subgrid-scale triggering energy, and stratiform instability in a toy tropical wave model. *J. Atmos. Sci.*, **57**, 1515–1535, doi:10.1175/1520-0469(2000)057<1515:CISSTE>2.0.CO;2.

- Moncrieff, M. W., and C. Liu, 2006: Representing convective organization in prediction models by a hybrid strategy. *J. Atmos. Sci.*, **63**, 3404–3420, doi:10.1175/JAS3812.1.
- Muller, C., L. Back, P. O’Gorman, and K. Emanuel, 2009: A model for the relationship between tropical precipitation and column water vapor. *Geophys. Res. Lett.*, **36**, L16804, doi:10.1029/2009GL039667.
- Neelin, J. D., O. Peters, J. W.-B. Lin, K. Hales, and C. E. Holloway, 2008: Rethinking convective quasi-equilibrium: Observational constraints for stochastic convective schemes in climate models. *Philos. Trans. Roy. Soc. London*, **A366**, 2581–2604, doi:10.1098/rsta.2008.0056.
- , —, and K. Hales, 2009: The transition to strong convection. *J. Atmos. Sci.*, **66**, 2367–2384, doi:10.1175/2009JAS2962.1.
- Nesbitt, S. W., R. Cifelli, and S. A. Rutledge, 2006: Storm morphology and rainfall characteristics of TRMM precipitation features. *Mon. Wea. Rev.*, **134**, 2702–2721, doi:10.1175/MWR3200.1.
- O’Gorman, P. A., and T. Schneider, 2006: Stochastic models for the kinematics of moisture transport and condensation in homogeneous turbulent flows. *J. Atmos. Sci.*, **63**, 2992–3005, doi:10.1175/JAS3794.1.
- , N. Lamquin, T. Schneider, and M. S. Singh, 2011: The relative humidity in an isentropic advection–condensation model: Limited poleward influence and properties of subtropical minima. *J. Atmos. Sci.*, **68**, 3079–3093, doi:10.1175/JAS-D-11-067.1.
- Peters, O., and J. D. Neelin, 2006: Critical phenomena in atmospheric precipitation. *Nat. Phys.*, **2**, 393–396, doi:10.1038/nphys314.
- , C. Hertlein, and K. Christensen, 2001: A complexity view of rainfall. *Phys. Rev. Lett.*, **88**, 018701, doi:10.1103/PhysRevLett.88.018701.
- , A. Deluca, A. Corral, J. D. Neelin, and C. E. Holloway, 2010: Universality of rain event size distributions. *J. Stat. Mech.*, **2010**, P11030, doi:10.1088/1742-5468/2010/11/P11030.
- Pierrehumbert, R. T., 1998: Lateral mixing as a source of subtropical water vapor. *Geophys. Res. Lett.*, **25**, 151–154, doi:10.1029/97GL03563.
- , H. Brogniez, and R. Roca, 2007: On the relative humidity of the earth’s atmosphere. *The Global Circulation of the Atmosphere: Phenomena, Theory, Challenges*, T. Schneider and A. H. Sobel, Eds., Princeton University Press, 143–185.
- Ratan, R., and V. Venugopal, 2013: Wet and dry spell characteristics of global tropical rainfall. *Water Resour. Res.*, **49**, 3830–3841, doi:10.1002/wrcr.20275.
- Redner, S., 2001: *A Guide to First-Passage Processes*. Cambridge University Press, 328 pp.
- Rickenbach, T. M., and S. A. Rutledge, 1998: Convection in TOGA COARE: Horizontal scale, morphology, and rainfall production. *J. Atmos. Sci.*, **55**, 2715–2729, doi:10.1175/1520-0469(1998)055<2715:CITCHS>2.0.CO;2.
- Roldán, J., and D. A. Woolhiser, 1982: Stochastic daily precipitation models: 1. A comparison of occurrence processes. *Water Resour. Res.*, **18**, 1451–1459, doi:10.1029/WR018i005p01451.
- Rossow, W. B., G. Tselioudis, A. Polak, and C. Jakob, 2005: Tropical climate described as a distribution of weather states indicated by distinct mesoscale cloud property mixtures. *Geophys. Res. Lett.*, **32**, L21812, doi:10.1029/2005GL024584.
- Schmitt, F., S. Vannitsem, and A. Barbosa, 1998: Modeling of rainfall time series using two-state renewal processes and multifractals. *J. Geophys. Res.*, **103** (D18), 23 181–23 193, doi:10.1029/98JD02071.
- Schumacher, C., and R. A. Houze Jr., 2003: Stratiform rain in the tropics as seen by the TRMM Precipitation Radar. *J. Climate*, **16**, 1739–1756, doi:10.1175/1520-0442(2003)016<1739:SRITTA>2.0.CO;2.
- , —, and I. Kraucunas, 2004: The tropical dynamical response to latent heating estimates derived from the TRMM precipitation radar. *J. Atmos. Sci.*, **61**, 1341–1358, doi:10.1175/1520-0469(2004)061<1341:TTDRTL>2.0.CO;2.
- Short, D. A., P. A. Kucera, B. S. Ferrier, J. C. Gerlach, S. A. Rutledge, and O. W. Thiele, 1997: Shipboard radar rainfall patterns within the TOGA COARE IFA. *Bull. Amer. Meteor. Soc.*, **78**, 2817–2836, doi:10.1175/1520-0477(1997)078<2817:SRPWT>2.0.CO;2.
- Sornette, D., 2004: *Critical Phenomena in Natural Sciences*. Springer Verlag, 528 pp.
- Stechmann, S. N., and A. J. Majda, 2009: Gravity waves in shear and implications for organized convection. *J. Atmos. Sci.*, **66**, 2579–2599, doi:10.1175/2009JAS2976.1.
- , and J. D. Neelin, 2011: A stochastic model for the transition to strong convection. *J. Atmos. Sci.*, **68**, 2955–2970, doi:10.1175/JAS-D-11-028.1.
- Steiner, M., R. A. Houze Jr., and S. E. Yuter, 1995: Climatological characterization of three-dimensional storm structure from operational radar and rain gauge data. *J. Appl. Meteor.*, **34**, 1978–2007, doi:10.1175/1520-0450(1995)034<1978:CCOTDS>2.0.CO;2.
- Sukhatme, J., and W. R. Young, 2011: The advection–condensation model and water-vapour probability density functions. *Quart. J. Roy. Meteor. Soc.*, **137**, 1561–1572, doi:10.1002/qj.869.
- Tulich, S. N., D. Randall, and B. Mapes, 2007: Vertical-mode and cloud decomposition of large-scale convectively coupled gravity waves in a two-dimensional cloud-resolving model. *J. Atmos. Sci.*, **64**, 1210–1229, doi:10.1175/JAS3884.1.
- Yano, J.-I., C. Liu, and M. W. Moncrieff, 2012: Self-organized criticality and homeostasis in atmospheric convective organization. *J. Atmos. Sci.*, **69**, 3449–3462, doi:10.1175/JAS-D-12-069.1.
- Yuter, S. E., R. A. Houze Jr., E. A. Smith, T. T. Wilheit, and E. Zipser, 2005: Physical characterization of tropical oceanic convection observed in KWAJEX. *J. Appl. Meteor.*, **44**, 385–415, doi:10.1175/JAM2206.1.